Inorganic Chemistry, Constable – Housecroft Group, Basel

New inorganic iridium(III) complexes for photonic applications

Master thesis for the *Master of Science in Nanosciences* at the University of Basel, Switzerland

Gabriel Schneider
01.09.2009

Table of contents

1. Introduction

We all live in a world, where the visual influences to our daily life are dominant. If you think, for example, of Las Vegas, the big and blazing advertising panels will appear clear in your mind. Until now these panels have consisted almost exclusively of solid state light emitting diodes (LED) made of doped silicon.

To explain the working principle of an LED made of doped silicon some theory must be described. An atom consists of a nucleus, made of positively charged protons, neutral neutrons and the negatively charged electrons, and in the Bohr model, the electrons are "circling around the nucleus". Electrons have discrete energy levels, but the huge numbers of atoms in a solid mean that the discrete energy levels of the electrons are split into bands. The energy levels in such a band are so close together that they are almost continuous. The different bands can be energetically very close to each other, far apart or overlap depending on the atoms in the solid. The lowest allowed energy levels are filled with electrons contributed by the atoms. The highest energy level containing electrons is known as the valence band. This band can be fully or partially filled with electrons, again depending on the atom.

With this knowledge it can be explained why some solids are conductors while others are insulators. If the valence band is only partially occupied, there are free energy levels within the band and the electrons can easily be transferred to the unoccupied levels under the influence of an electric field. Therefore this material is a good conductor. If the valence band is completely filled and the conducting band is at a much higher energy level, the applied electric field is not strong enough to transfer electrons to the conducting band. This material is therefore an insulator. In a conductor, the valence band is only partially filled and therefore the valence band is also the conducting band. The energy gap between the bands is called the band gap.

Sometimes the band gap is only very small (e.g. 1.10 eV for silicon). In this case, at 0 K the valence band is completely filled while the conducting band is empty. At room temperature some electrons are in the conducting band due to their thermal energy. Such a material is called a semi-conductor. Semi-conductors have the interesting behaviour that the specific resistance decreases with increasing temperature in contrast to a metallic conductor. At higher temperatures more electrons are raised to the conducting band, thus reducing the resistance. With each electron raised to a higher level a positively charged hole is left in the valence band.

Figure 1 shows four possible band structures. The first conductor has a partly filled valence band. The electrons can be excited into the energy level directly above. The second conductor has an overlap of the allowed energy bands. The insulator has a big band gap between the completely occupied valence band and the empty conducting band. In the semi-conductor this band gap between the completely occupied valence band and the empty conducting band is very small. Therefore some electrons can be excited into the conducting band even at room temperature, thus leaving behind positively charged holes.
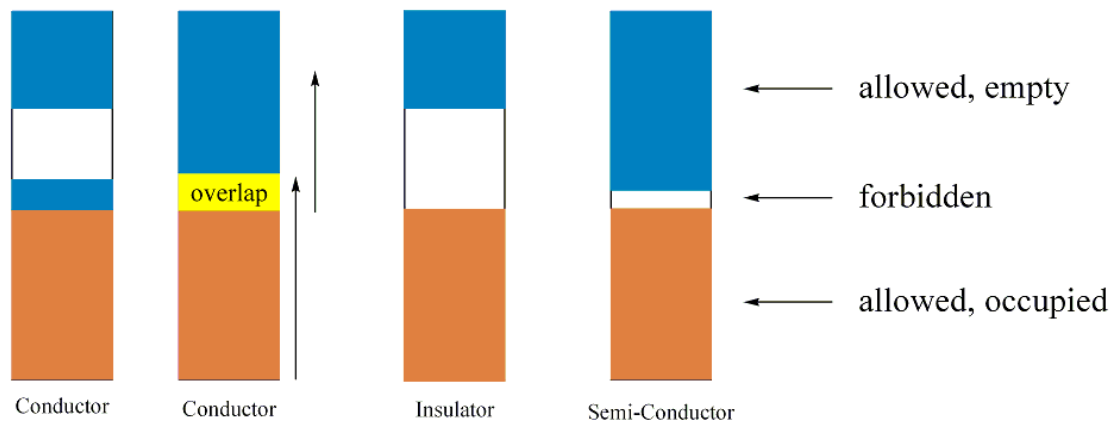
Figure 1: Different possible band structures of conductors, insulators and semi-conductors. The allowed and occupied levels are orange, the forbidden levels white and the allowed and empty levels blue. The yellow part is an overlap of the valence and the conducting band.

For a working LED, silicon must be doped with other atoms like gallium and arsenic. Silicon has four valence electrons, arsenic five and gallium three. Therefore the substitution of a silicon atom with an arsenic atom means adding one valence electron. Four electrons of the arsenic are used for the covalent bonds to the four surrounding silicon atoms. The fifth valence electrons of arsenic occupy energy levels just below the conducting band and thus can be easily raised into the conducting band resulting in electrical current. These energy levels are called donor levels. The process of adding an electron in this way is called negative doping or n-doping of silicon and there are no holes created in the valence band.

Another semi-conductor type is formed by substituting some silicon atoms with gallium. Gallium has only three valence electrons which are all used for covalent bonds to the four surrounding silicon atoms. The missing electron can also be regarded as a "hole" with a positive charge. Hence we are talking about a positive doping of silicon or abbreviated p-doped silicon. The holes yield some additional empty energy levels just above the valence band. These levels are called acceptor levels, because of the ease in raising electrons from the valence band into these acceptor levels.
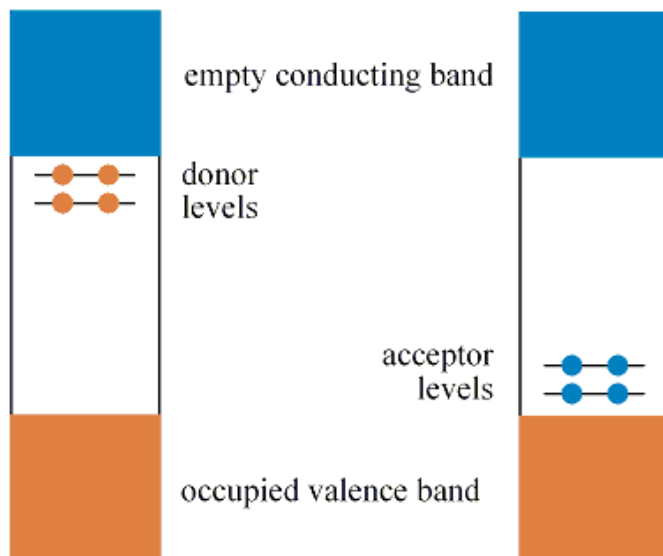
In Figure 2 the donor and acceptor levels are drawn. The acceptor levels are empty like the conducting band while the donor levels are filled with electrons like the valence band.

Figure 2: Schematic donor and acceptor levels.

The main component of an LED is the contact between a negatively and a positively doped semi-conductor. Connecting the anode to the positively doped side and the cathode to the negatively doped side and applying a current, leads to the diffusion of the holes and electrons will be increased and current flows yielding emission of light (see below). If the anode is connected to the negatively doped side and the cathode to the positive side no current will flow. The light of the LEDs results from the release of a photon if an electron meets a hole and therefore reduces its energy. When the voltage is applied to a pure silicon crystal, no photons will be released because the diffusion of holes and electrons is only very low. Therefore the silicon must be doped. The colour of the light depends on the band gap, which in turn depends on the elements used.[4-11]

Back to Las Vegas and the advertising panels. Solid state LEDs also have many other applications, not to say much more useful tasks. They have already been in use for quite some time in the computer industry. They are used in pocket lights and in mobile phones. And today you can substitute not only the rear lights but also the headlamps of some cars with LEDs. They are already well-established in bicycle lights. The main advantages of LEDs compared to halogen bulbs are their low power consumption, longer lifetimes, higher shock resistance and higher light yield.

Due to the huge research effort in the last fifty years, today we can buy LEDs with all colours and they are the most common electroluminescent devices. But the solid state LEDs also have disadvantages. The fabrication results in high energy consumption and therefore involves high costs due to the necessity for high temperatures and vacuum conditions for the controlled growth of the single crystals of doped silicon. The white light of LEDs has no continuous spectrum like sunlight, because the LEDs have almost monochromatic spectra.

For some years there have been alternatives to LEDs in the form of organic light emitting diodes (OLEDs). An OLED consists of a thin film with electroluminescent behaviour sandwiched between two electrodes. At least one of the electrodes must be transparent to allow photons to pass through. The main difference to a LED is the absence of single crystals. The film is made of organic semi-conducting materials with lower light and current density. OLEDs have a much better contrast and are brighter than LEDs.

The organic layer is mostly made of undoped and insulating molecules which have intermolecular π-stacking interactions or form polymers. The molecules are uncharged and therefore the charges needed for the working of an OLED are injected into the organic layer at the electrodes. The cathode should have a low minimum energy needed to remove an electron from an uncharged solid. This is called a low work function. The cathode injects the electrons into the organic layer. In contrast, the anode should have a high work function.

The electrons injected from the cathode and the holes (positive charges) injected from the anode drift to the other pole in the device due to the applied electric field. The requirement for drifting needs a strong electric field and therefore the devices need to be very thin to be able to run them at low voltages. If an electron and a hole meet in the organic layer, they neutralize each other. With an appropriate material this

neutralization releases a photon. The emitted wavelength also depends on the material.
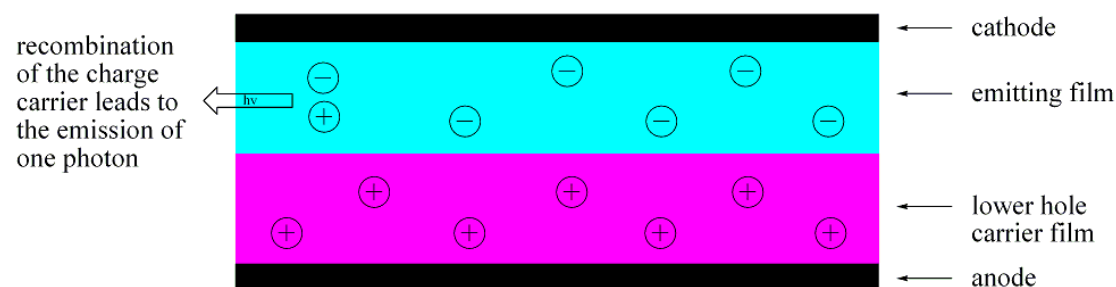
The working scheme of an OLED is shown in Figure 3.

Figure 3: Scheme of an OLED

But what is the basis for the huge research effort to find out new devices as successors for the well-established silicon-based LEDs? LEDs incorporate single crystals of p- and n-doped silicon. These single crystals are expensive to produce. A bigger advantage of OLEDs in comparison to LEDs is that they allow the fabrication of very thin and flexible devices. They are therefore under intensive investigation because they can be used for flexible screens, for room lighting and for displays printed on fabric or clothes. There are already a few OLED displays in use, for example in displays in digital cameras or in small computer screens. They have much better contrast, are brighter, have a wider viewing angle and the power consumption is much lower compared to common flat screens. The main problem today is the limited lifetime of the organic materials. The different stabilities of the organic molecules used can result in colour changes during the lifetime of an OLED screen.

Although OLEDs are not yet widely used, there is already considerable research into a possible successor, namely the light emitting electrochemical cells, abbreviated LEEC or LEC. A LEEC has a significantly simplified architecture compared to an OLED. The two electrodes again sandwich the emissive layer containing the light emitting molecules. In this application the emitting molecules need to be ionic. Compared to an OLED, LEECs are independent of the work function of the electrodes. While the OLED needs a perfect encapsulation to prevent the degradation of the electron-injecting layers, air-stable electrodes like gold, silver can be used with LEECs.

A LEEC is cheaper to produce due to its simpler architecture and is much more robust than an OLED. It needs no high vacuum conditions and consists of a "single active layer composed of an ionic transition-metal complex (iTMC)". [1] They are easy to fabricate, but currently, the main problem similar to OLEDs is the short lifetime of the cells. These range from only a few minutes of luminescence to a few thousand hours. At present, research is focused on increasing the range of colours and improving the lifetimes with the aim of applying LEECs in, for example, computer screens, TVs, room lightning, etc.

Ongoing from my last project work in the group of *Professor Dr. Edwin Constable* and *Professor Dr. Catherine Housecroft* and from the doctoral thesis of *Stefan Graber* on the same topic, the aim of the work described here was to synthesize new iridium(III) complexes for photonic devices. Since these iridium complexes consist of charged ions there are, in principle, two ways to produce new electrochemical devices

based on iridium(III). The ligands around the iridium metal centre can be changed or an electroluminescent counterion can be used to form the charged complex. In this work, both ways were followed. Firstly, different ligands were used to form complexes with the non-luminescent counterion $[PF_6]^-$. Then, trials were done to form a luminescent molecule to use it as counterion instead of $[PF_6]^-$. This was tried using the well-known and strongly emitting ruthenium(II) bipyridine carboxylic acid derivatives. These syntheses consumed most of the time working in the laboratory but unfortunately they did not give any useful results. Due to different problems in the synthesis, this method was not successful and therefore finally due to lack of time not investigated further.

The most successful achievement of the project was the synthesis of an iridium(III) complex which was a dual emitter. A dual emitter has two simultaneous emissions at different wavelengths. The idea of a dual emitter is to get new colours. If you overlay two different shining colours, you will get a new colour. And if you take the right wavelengths the emission appears to be white. The white sunlight is an overlay of the whole visible spectrum. This can be proved with a simple optical prism. Therefore two colours resulting in white light is the simplest approach. If the two emitted colours are not appropriate to give white light, they will still give another, hopefully new, colour.

With the last synthesis, inspired by the PhD presentation of *Stefan Graber,* a most interesting iridium complex was found, which exhibited the desired dual emission. This complex is still under investigation in the group of *Dr. Henk Bolink* at the *University of Valencia* in Spain.[1],[4]

The metal centre used was an iridium(III) ion. Iridium (group 9), with atomic number 77, is very hard, lustrous, silver-coloured and unreactive. Iridium and osmium are the densest elements known and both belong to the platinum group metals. Iridium is one of the least abundant elements of the Earth's crust, even less abundant than gold or platinum. Iridium was discovered along with osmium by *Smithson Tennant* in 1803, and its name means "prismatic colours" in Greek *("iridios")* due to the many colours of its compounds. The iridium complexes synthesized in this work also show many different colours (see Figure 12).

The known oxidation states of iridium are from -1 to +6, the most stable are +3 and +4. In the synthesized complexes, the oxidation state is +3, resulting in a *[Xe] $5d^6$* electron configuration. for an octahedral metal centre, a *d^6* electron configuration for a 2nd or 3rd row metal ion is invariably low-spin, which means the electrons are paired, and the complexes are kinetically inert with diamagnetic properties.

The main property of the complexes synthesized in this master thesis is the photoluminescence (abbreviated as PL). PL is the process by which an electron of the highest occupied molecular orbital (HOMO) will be excited via the incoming photons to the lowest unoccupied molecular orbital (LUMO) as shown below in Figure 4.
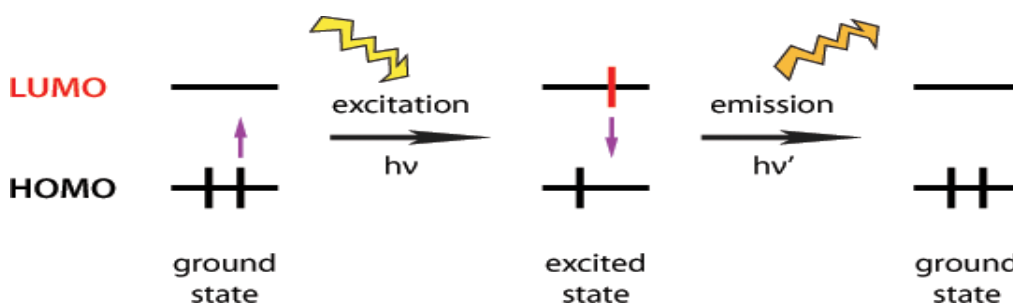
Figure 4: The principles of photoluminescence. Image is taken from the PhD Thesis of S. Graber with the permission of the author.

The incoming photon excites the electron to a higher energy level (LUMO). When the electron returns to the ground state (HOMO), a photon will be released which results in the observable emission. Due to thermal and vibrational losses, the observed emission is at lower energy than the excitation, hence the wavelength of the emission is longer which leads to a red shift.

In general the process in LEDs, OLEDs and LEECs is called solid state lighting. In a LEEC the cathode transfers electrons on to the metal complexes and at the anode the electrons are withdrawn from the molecules. If two differently charged molecules meet, the electron is transferred to neutralise the charge difference and hence a photon is emitted. The sum of this process, named electroluminescence (EL), over lots of molecules results in the emission of visible light. This process is shown below in Figure 5.
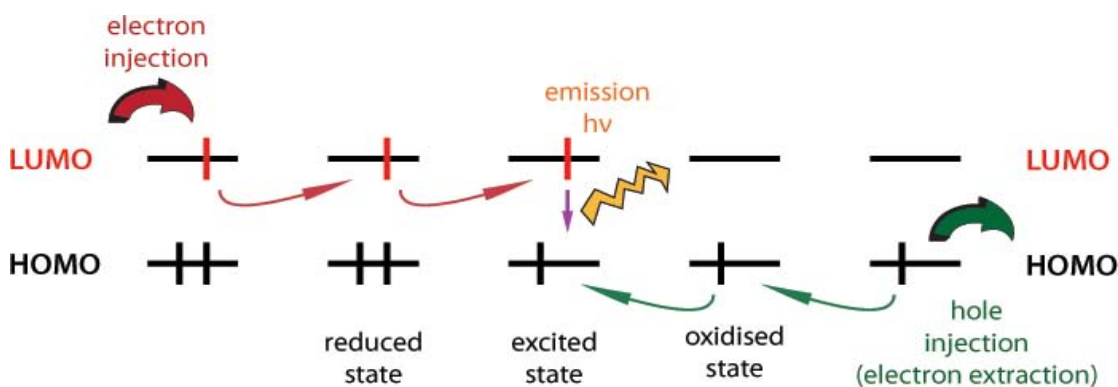

Figure 5: The principles of electroluminescence. Image is taken from the PhD Thesis of S. Graber with the permission of the author.

In contrast an OLED has a more complicated structure. They consist of one or more organic layers in a sandwiched structure between two electrodes. One of the electrodes must be transparent to allow photons to pass through.[27],[29]

8

2. Materials and Methods

The ligands, donated from *P. Rösel* from our group, and the fluorinated iridium(III) precursor, donated from *S. Graber* also from our group, were used without further purification. All other used chemicals were commercially available in reagent grade and were also used without further purification.

Fluka silica gel 60 and Merck aluminium oxide 90 respectively were used for column chromatography. The solvents were freshly distilled before use.

Most of the syntheses were done in the microwave reactor (Biotage Initiator 8 with a maximum power of 400 W).

The ^{1}H and ^{13}C NMR spectra were measured on Bruker AM250 (250 MHz), Bruker DRX400 (400 MHz), Bruker DRX500 (500 MHz) and Bruker DRX600 (600 MHz) spectrometers.

Electrospray ionization mass spectra (abbreviated with ESI-MS) were recorded either by *P. Rösel* or *R. Schmitt* on a Bruker Esquire 3000 plus instrument at 250 °C. FAB mass spectra were performed on a Finnigan MAT 95Q apparatus by *P. Nadig*. Elemental analyses were measured with a Leco CHN-900 microanalyser by *W. Kirsch*.

An Agilent Chemstation 8453 Spectrophotometer was used for the UV-Visible absorption measurements. The fluorescence of iridium(III) complexes was performed on a Shimadzu RF-5301PC spectrofluorometer. The wavelengths for the excitation for the fluorescence measurements were selected according to the absorption measurements. The excitation and emission slits were kept on 3.0 or 5.0 units respectively.

The crystal structures were resolved by *J. Zampese* on a Stoe IPDS diffractometer, using Stoe IPDS software[12] and SHELXL97[13] software for the data reduction, solution and refinement, and *M. Neuburger* on a Bruker – Nonius Kappa CCD diffractometer (graphite monochromated MoKα radiation) using the programs COLLECT[14], SIR92[15], DENZO/SCALEPACK[16] and CRYSTALS[17] were used by *M. Neuburger*. For visualization and structural analyses the software CCDC Mercury (version 2.2)[18] was used.

An Eco Chemie Autolab PGSTAT 20 was used for the electrochemical measurements. Glassy carbon was used as working electrode, a platinum mesh for the counter electrode, and a silver wire as the reference electrode. The redox potentials were determined by cyclic voltammetry (CV) and by square wave (SW). The compounds were dissolved and measured in dry acetonitrile in the presence of 0.1 M [*n*-Bu$_4$N][PF$_6$]. The scanning rate for the CV was 100 mVs^{-1} in all cases and ferrocene (Fc) was added as an internal standard at the end of every experiment.

3. Experimental

In the following part the syntheses are described. In Chapter 4 in Scheme 1 is an overview of the complexation reactions. The ligands are shown in Figure 6. All ligands were synthesized by *P. Rösel* during his PhD studies and were used without further purifications.
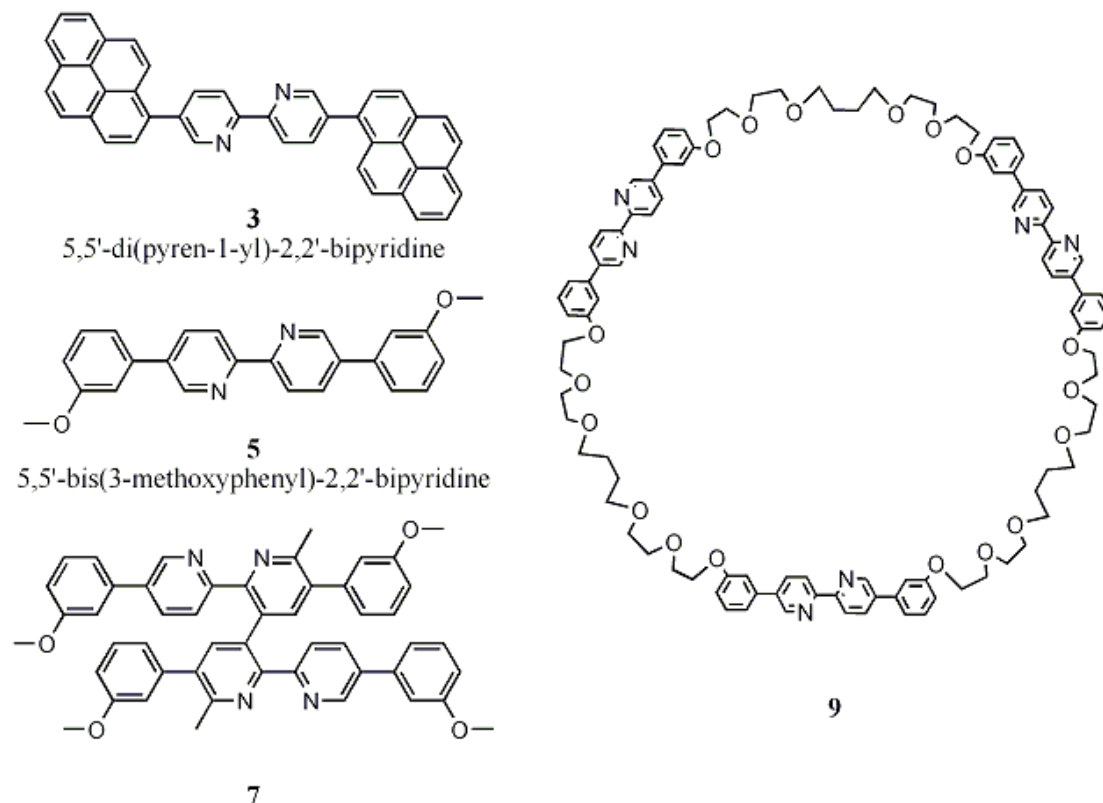

3
5,5'-di(pyren-1-yl)-2,2'-bipyridine

5
5,5'-bis(3-methoxyphenyl)-2,2'-bipyridine

7

9

Figure 6: Ligands used for complexation

Synthesis of tetrakis(2-phenylpyridine-C,N)di(µ-chloro)diiridium(III) (2)

Iridium trichloride hydrate (IrCl$_3$*6H$_2$O, 2.0 g, 4.9 mmol) was combined with 2-phenylpyridine (3.9 g, 25 mmol), dissolved in a mixture of 2-ethoxyethanol (155 mL, distilled over MgSO$_4$) and water (52 mL) and refluxed for 24 hours. The solution was cooled to room temperature and the yellow precipitate was collected on a glass filter frit. The precipitate was washed with 95 % ethanol (310 mL) and acetone (310 mL) and then dissolved in CH$_2$Cl$_2$ (approximately 600 mL) and filtered. Toluene (130 mL) and hexane (52 mL) were added to the filtrate, which was then reduced in volume by evaporation to 50 ml and cooled to give yellow-green crystals of tetrakis(2-phenylpyridine-C,N)di(µ-chloro)diiridium(III) abbreviated as [Ir(ppy)$_2$Cl]$_2$ (**2**).[2],[3]

 Yield: 0.60 g, 0.56 mmol, 11.4 %

[1]**H NMR** (400 MHz, CD$_2$Cl$_2$) δ = 9.25 (d, *J* = 5.0 Hz, 1H), 7.94 (d, *J* = 7.9 Hz, 1H), 7.80 (td, *J* = 7.8 Hz, 1.5, 1H), 7.56 (dd, *J* = 7.8 Hz, 1.1, 1H), 6.83 (m, 2H), 6.60 (td, *J* = 7.8 Hz, 1.3, 1H), 5.87 (dd, *J* = 7.8 Hz, 0.8, 1H).[4]

Synthesis of compound 4

A grey-green suspension of [Ir(ppy)$_2$Cl]$_2$ (61.2 mg, 0.0571 mmol, **2**) and 5,5'-di(pyren-1-yl)-2,2'-bipyridine (63.9 mg, 0.115 mmol, **3**) in methanol (7 mL) and dichloromethane (7 mL) was refluxed under an inert atmosphere of nitrogen in the dark for 10 hours. In the morning nothing has changed, the colour was still grey-green and thin-layer chromatography (TLC) showed no reaction.
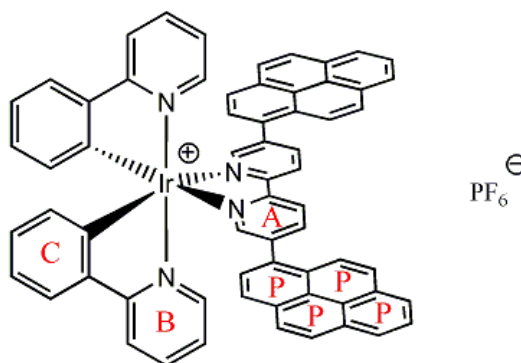

Figure 7: Scheme of Compound 4 with the NMR labels in red.

The reaction conditions were changed. The mixture was heated at 110 °C in a microwave reactor at a pressure between 9 and 14 bar. After 1 hour, the colour had changed to a clear olive-green. An excess of ammonium hexafluorophosphate was added and the solution was stirred for 90 minutes. After filtration the residue was washed with methanol. The colour of the powder was red-brown. The powder was cleaned on a short silica gel column with dichloromethane – methanol (100:2) as eluent.

The crude solid was recrystallised from dichloromethane layered with diethyl ether. After standing overnight, some bright orange crystals had formed but they were too small for X-ray diffraction analysis. Therefore the salt was purified on an Alox 90 column with the eluent dichloromethane to methanol (100:2) yielding 100 mg of the dried orange powder (100 mg, 0.0832 mmol, 72.3 %). X-ray quality crystals were grown over three days by layering a dichloromethane solution of the complex with diethyl ether.

Yield: 100 mg, 0.0832 mmol, 72.3 %

^{1}H NMR (500 MHz, DMSO) δ/ppm 9.25 (d, J = 8.4 Hz, 1H, H$^{3(A)}$), 8.69 (d, J = 8.3 Hz, 1H, H$^{4(A)}$), 8.54 (d, J = 8.2 Hz, 1H, H$^{3(B)}$), 8.43 (t, J = 6.9 Hz, 2H, H$^{(P)}$), 8.40 (d, J = 7.8 Hz, 1H, H$^{(P)}$), 8.30 (d, J = 8.9 Hz, 1H, H$^{(P)}$), 8.26 (t, J = 8.8 Hz, 2H, H$^{5(B)}$+H$^{(P)}$), 8.19 (d, J = 1.8 Hz, 2H, H$^{6(A)}$+H$^{(P)}$), 8.17 (d, J = 4.9 Hz, 1H, H$^{6(B)}$), 8.11 (t, J = 7.8 Hz, 1H, H$^{4(B)}$), 8.07 (d, J = 7.8 Hz, 1H, H$^{(P)}$), 7.98 (d, J = 7.7 Hz, 1H, H$^{6(C)}$), 7.55 (d, J = 9.2 Hz, 1H, H$^{(P)}$), 7.32 (t, J = 6.6 Hz, 1H, H$^{5(B)}$), 6.74 (t, J = 7.4 Hz, 1H, H$^{5(C)}$), 6.69 (t, J = 7.3 Hz, 1H, H$^{4(C)}$), 6.28 (d, J = 7.4 Hz, 1H, H$^{3(C)}$). **MS** (ESI, m/z) 1057.2 [M − PF$_6$]$^+$ (calc. 1057.25). **Calcd.** for C$_{64}$H$_{40}$N$_4$IrPF$_6$ (1202.21) C 63.94, H 3.35, N 4.66; found C 65.70, H 4.51, N 3.72 %.

Synthesis of compound 6

A grey-green suspension of [Ir(ppy)$_2$Cl]$_2$ (61.2 mg, 0.057 mmol, **2**) and 5,5'-bis(3-methoxyphenyl)-2,2'-bipyridine (42.4 mg, 0.115 mmol, **5**) in methanol (5 mL) was heated at 120 °C in the microwave reactor for 40 minutes at a pressure of 14 bar. The starting green-yellowish color of the mixture changed to a bright orange.

An excess of ammonium hexafluorophosphate was added and the solution was stirred for 60 minutes. A precipitate was visible. The methanol was reduced in volume and distilled water was added which resulted in an orange precipitate. After filtration the

residue was washed with water and diethyl ether yielding a bright orange solid (mass of the impure solid: 104.4 mg)

The crude solid was dissolved in dichloromethane and layered with diethyl ether but no crystals grew over two weeks. Therefore the salt was purified on an Alox 90 column with the eluent dichloromethane – methanol (100:2) yielding 52.1 mg of a dried orange powder (52.1 mg, 0.0514 mmol, 44.7 %). Orange crystals were grown in the fridge over 10 days from an acetonitrile solution of the complex into which diethyl ether vapour diffused.
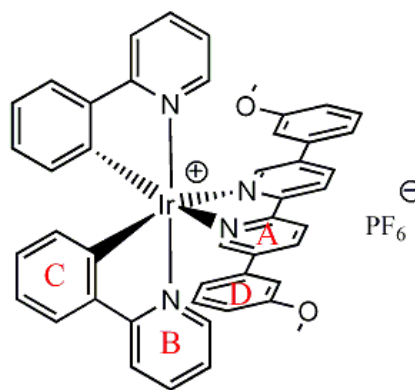

Figure 8: Scheme of compound 6 with the NMR labels in red.

Yield: 52.1 mg, 0.0514 mmol, 44.7 %

^{1}H NMR (500 MHz, DMSO) δ/ppm 8.98 (d, J = 8.5 Hz, 1H, H$^{3(A)}$), 8.62 (d, J = 8.4 Hz, 1H, H$^{4(A)}$), 8.29 (d, J = 8.2 Hz, 1H, H$^{3(B)}$), 8.05 (s, 1H, H$^{6(A)}$), 7.98 (d, J = 7.8 Hz, 1H, H$^{6(C)}$), 7.94 (t, J = 7.8 Hz, 1H, H$^{4(B)}$), 7.85 (d, J = 5.7 Hz, 1H, H$^{6(B)}$), 7.39 (t, J = 8.0 Hz, 1H, H$^{5(D)}$), 7.17 (t, J = 6.6 Hz, 1H, H$^{5(B)}$), 7.07 (t, J = 7.5 Hz, 1H, H$^{5(C)}$), 7.02 (d, J = 7.9 Hz, 2H, H$^{4(D)}$+H$^{6(D)}$), 6.97 (t, J = 7.5 Hz, 1H, H$^{4(C)}$), 6.89 (s, 1H, H$^{2(D)}$), 6.33 (d, J = 7.5 Hz, 1H, H$^{3(C)}$), 3.75 (s, 3H, CH$_3$). **MS** (ESI, m/z) 868.8 [M – PF$_6$]$^+$ (calc. 869.02). **Calcd.** for C$_{46}$H$_{36}$N$_4$O$_2$IrPF$_6$ (1202.21) C 54.49, H 3.58, N 5.53; found C 54.58, H 3.58, N 5.24 %.

Synthesis of compound 8

A grey-green suspension of [Ir(ppy)$_2$Cl]$_2$ (61.2 mg, 0.0571 mmol, **2**) and ligand **7** (44.0 mg, 0.0576 mmol, **7**) in methanol (5 mL) was heated at 120 °C in the microwave reactor for 40 minutes at a pressure of 14 bar. The green-yellow colour of the mixture changed to bright red.
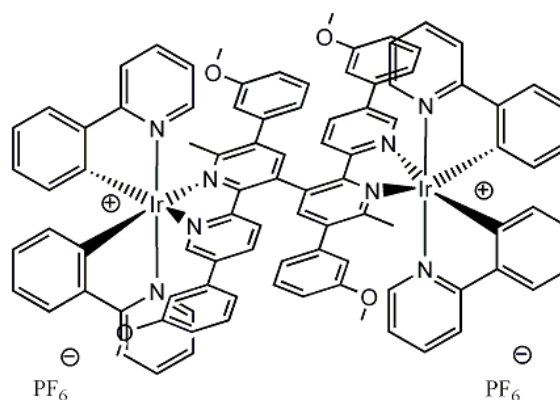

Figure 9: Scheme of compound 8

The methanol was reduced in volume and ammonium hexafluorophosphate dissolved in distilled water was added and the mixture was stirred for 30 minutes. While adding the water, the solution changed its colour from red to pale orange. After filtration the residue was washed with water and diethyl ether yielding a pale orange solid (mass of the impure solid: 121.3 mg)

The crude solid was dissolved in dichloromethane layered with diethyl ether but no crystals grew over two weeks. Therefore the salt was purified on an Alox 90 column with the eluent dichloromethane – methanol (100:2) yielding 77.6 mg of a dried orange powder (77.6 mg). Orange crystals were grown in the fridge from an acetonitrile solution of the complex into which diethyl ether vapour diffused, but unfortunately they were arranged like the spines of a hedgehog and were unsuitable for X-ray analysis.
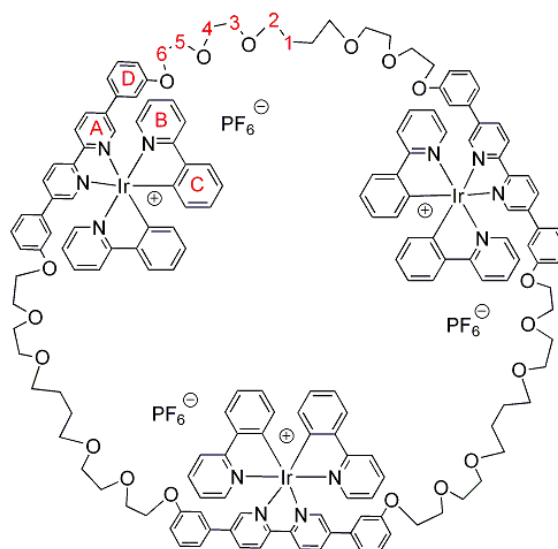
Yield: 77.6 mg (mixture)

MS (ESI, *m/z*) 501.1 [IrC$_{22}$N$_2$H$_{16}$] (calc. 500.59), 881.8 [M – 2PF$_6$]$^{2+}$ (calc. 882.04), 1262.9 [M – PF$_6$ – IrC$_{22}$N$_2$H$_{16}$] (calc. 1263.49), 1908.9 [M – PF$_6$]$^+$ (calc. 1909.04). **Calcd.** for C$_{94}$H$_{74}$N$_8$O$_4$Ir$_2$P$_2$F$_{12}$ (2053.99) C 54.97, H 3.63, N 5.46; found C 54.78, H 3.74, N 5.44 %.

^{1}H NMR: all NMR spectra are (see discussion and appendix).

Synthesis of compound 10

A grey-green suspension of [Ir(ppy)$_2$Cl]$_2$ (31.0 mg, 0.0289 mmol, **2**) and cyclo-tri-5,5'-di(pyren-1-yl)-2,2'-bipyridine (33.0 mg, 0.0193 mmol, **9**) dissolved in dichloromethane (1 mL) was heated in methanol (5 mL) in the microwave reactor at 110 °C for 40 minutes at a pressure of 14 bar. The green-yellow colour of the mixture changed to orange.

All the dichloromethane was evaporated and the methanol was reduced in volume. Distilled water was added which resulted in an immediately color

Figure 10: Scheme of compound 10 with the NMR labels in red.

change from orange to milky white-orange. An excess of ammonium hexafluorophosphate was added and the solution was stirred for 60 minutes. After filtration, the residue was washed with water and diethyl ether yielding an orange solid (mass of the impure solid: 128.0 mg).

The crude solid was dissolved in dichloromethane in an environment of saturated diethyl ether vapour but no crystals grew. Therefore the salt was purified on an Alox 90 column with the eluent being dichloromethane to methanol (100:2) yielding 48 mg of a dried orange powder (48.0 mg). Several setups for crystallisation were tried, acetonitrile with diethyl ether, dichloromethane with diethyl ether, dichloroethane with diethyl ether, dichloroethane with ethyl acetate but no crystals could be grown over 6 weeks, neither at room temperature nor in the fridge.

Yield: 48 mg (mixture)

MS (ESI, *m/z*) 1070.9 [M – 3PF$_6$]$^{3+}$ (calc. 1071.27), 1355.8 [M – 2PF$_6$ – IrC$_{22}$N$_2$H$_{16}$]$^{2+}$ (calc. 1356.61), 1678.6 [M – 2PF$_6$]$^{2+}$ (calc. 1679.39). **Calcd.** for C$_{168}$H$_{162}$N$_{12}$O$_{18}$Ir$_3$P$_3$F$_{18}$ (3648.68) C 55.30, H 4.48, N 4.61; found C 54.73, H 4.73, N 4.16 %.

^{1}H NMR: all NMR spectra are complex and shown in the appendix. The five CH$_2$-groups from the linking ether groups can be seen between 3.97 and 3.34 ppm and the CH$_2$$^{(1)}$ is at 1.47 ppm. (Part of the **^{1}H NMR** (500 MHz, CD3CN) δ/ppm = 3.97 (s, 1H), 3.72 (s, 1H), 3.57 (s, 1H), 3.47 (s, 1H), 3.34 (s, 1H), 1.47 (s, 1H).)

Synthesis of the dual emitter compound 12

A yellow suspension of [Ir(L)$_2$Cl]$_2$ (69.3 mg, 0.0570 mmol, **11**, HL = 2-(2,4-difluorophenyl)pyridine) and 5,5'-di(pyren-1-yl)-2,2'-bipyridine (63.9 mg, 0.115 mmol, **3**) in methanol (5 mL) was heated in the microwave reactor at 120 °C for 1 hour at a pressure of 14 bar. The bright yellow colour changed to green-yellow with a black precipitate. The mixture was heated for a further 30 minutes at 140 °C under a pressure of 22 bar. An excess of ammonium

Figure 11: Scheme of compound 12 with the NMR labels in red.

hexafluorophosphate was added and the mixture was stirred for 30 minutes. After filtration, the residue was washed with water and diethyl ether yielding a green-yellow solid.
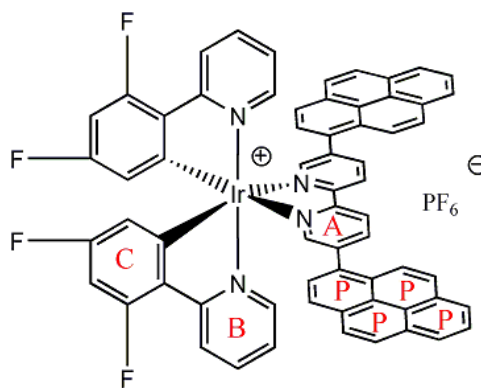
The salt was purified on a short silica gel column with the eluent being dichloromethane – methanol (10:1) yielding 143 mg of a yellow (slightly orange) solid (143 mg, 0.112 mmol, 97.6 %)

The crude solid was recrystallised at room temperature from dichloroethane into which diethyl ether vapour was allowed to diffuse. After 5 days there were orange crystals with excellent X-ray quality. 50 mg of the compound were sent to Valencia (Spain) to *Dr. Henk Bolink* for further investigation in LEECs and OLEDs.

Yield: 143 mg, 0.112 mmol, 97.6 %

^{1}H NMR (500 MHz, CD2Cl2) δ/ppm 8.86 (d, J = 8.0 Hz, 1H, H$^{3(A)}$), 8.57 (d, J = 7.5Hz, 1H, H$^{4(A)}$), 8.54 (d, J = 8.7 Hz, 1H, H$^{3(B)}$), 8.41 (s, 1H, H$^{6(A)}$), 8.31 (d, J = 7.6 Hz, 3H, H$^{(P)}$), 8.21 (d, J = 8.9 Hz, 1H, H$^{(P)}$), 8.14 (dd, J = 13.4 Hz, 6.5 Hz, 3H, H$^{(P)}$), 8.01 (t, J = 8.0 Hz, 1H, H$^{4(B)}$), 7.98 (d, J = 8.0 Hz, 1H, H$^{(P)}$), 7.91 (d, J = 5.6 Hz, 1H, H$^{6(B)}$), 7.68 (d, J = 9.1 Hz, 1H, H$^{(P)}$), 7.24 (t, J = 6.4 Hz, 1H, H$^{5(B)}$), 6.38 (t, J = 10.7 Hz, 1H, H$^{4/6(C)}$), 5.80 (d, J = 8.2 Hz, 1H, H$^{6/4(C)}$). **MS** (ESI, m/z) 1128.5 [M – PF$_6$]$^+$ (calc. 1129.21). **Calcd.** for C$_{168}$H$_{162}$N$_{12}$O$_{18}$Ir$_3$P$_3$F$_{18}$ + 5CH$_2$Cl$_2$ (1698.83) C 48.78, H 2.72, N 3.30; found C 48.71, H 2.55, N 3.32 %.

4. Results and Discussion

4.1 Synthesis and analysis
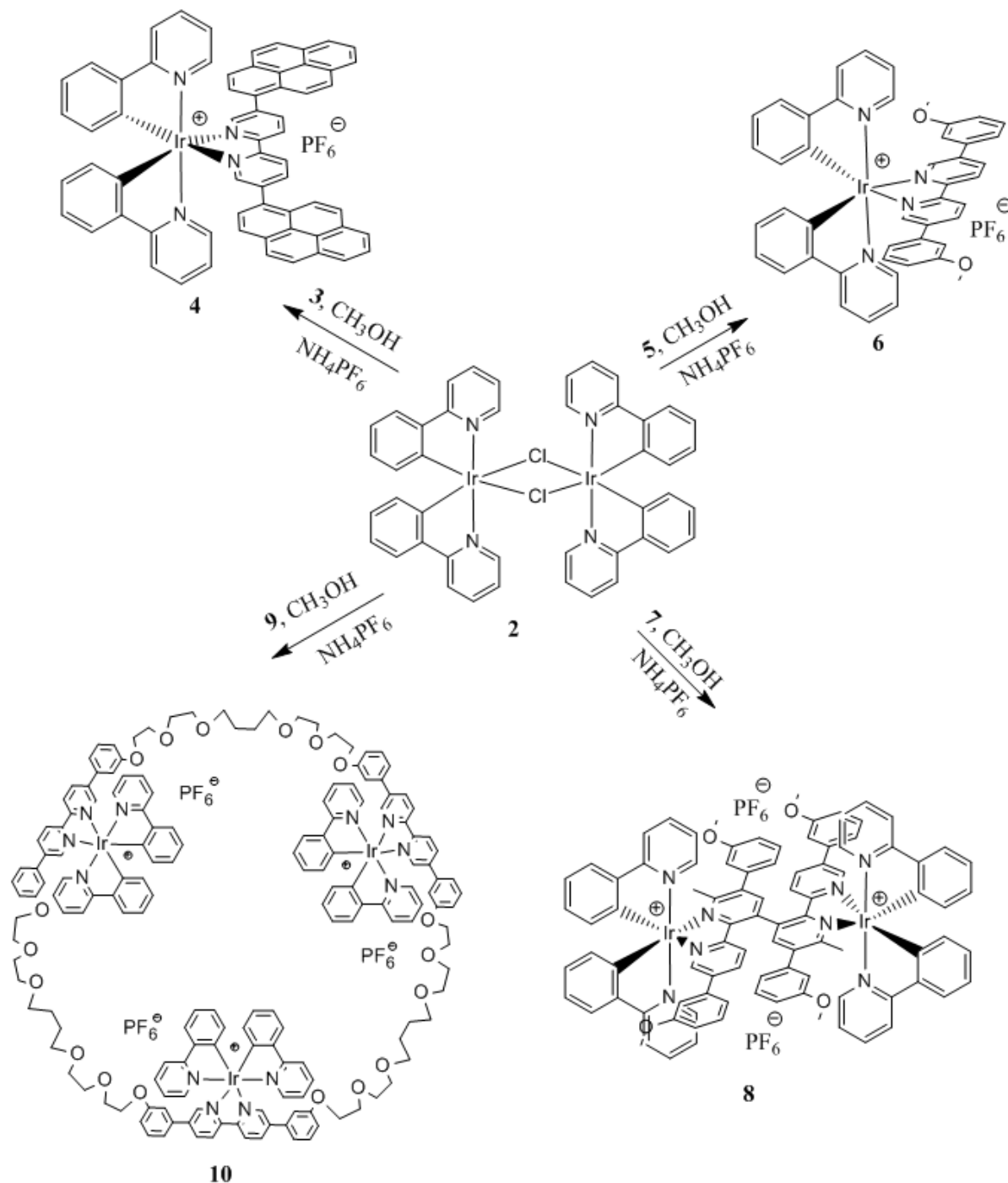
Scheme 1: Overview of the iridium(III) complexes starting from tetrakis(2-phenylpyridine-C,N)di(μ-chloro)di-iridium(III) (abbreviated as [Ir(ppy)₂Cl]₂, (2)).

15

The large scale synthesis of compound **2** unfortunately resulted in a very poor yield. The main problem was the growing of the crystals, namely the right proportion of the three required solvents. However, the amount of compound **2** obtained was far more than needed for this work and therefore no further trials do improve the yield were done. The ^{1}H NMR spectrum agreed with the data of *S. Graber* and no other analyses were done. An overview of the iridium(III) compounds based on compound **2** are shown in Scheme 1.

The first complexation reaction to form compound **4** was tried according to the procedure of *S. Graber*. After refluxing the mixture for one night, there was neither a visible change of colour of the mixture nor in the TLC, the reaction was tried in the microwave reactor. Due to the success of this attempt, further iridium(III) compounds were synthesized directly in the microwave reactor without prior refluxing. This accelerated the synthesis by reducing the reaction time from 12 hours to one hour or less. If needed, the mixtures were heated several times in the microwave reactor. The progress of the reaction was checked by TLC. The yields of the complexation steps were between 45 and 98% which is good given the fact that the ligands were not always completely pure and were sometimes poorly soluble.

As mentioned in the introduction the iridium complexes stand out with their variety of colours. The starting iridium trichloride hydrate is black, compound **2** is yellow-green while the iridium(III) complexes have red-orange colours. In Figure 12, the synthesized complexes and their structures are shown. In all the iridium(III) complexation reactions the change of colour of the mixture during the reaction was visible to the naked eye. Another visible observation was the colour change after adding the ammonium hexafluorophosphate.
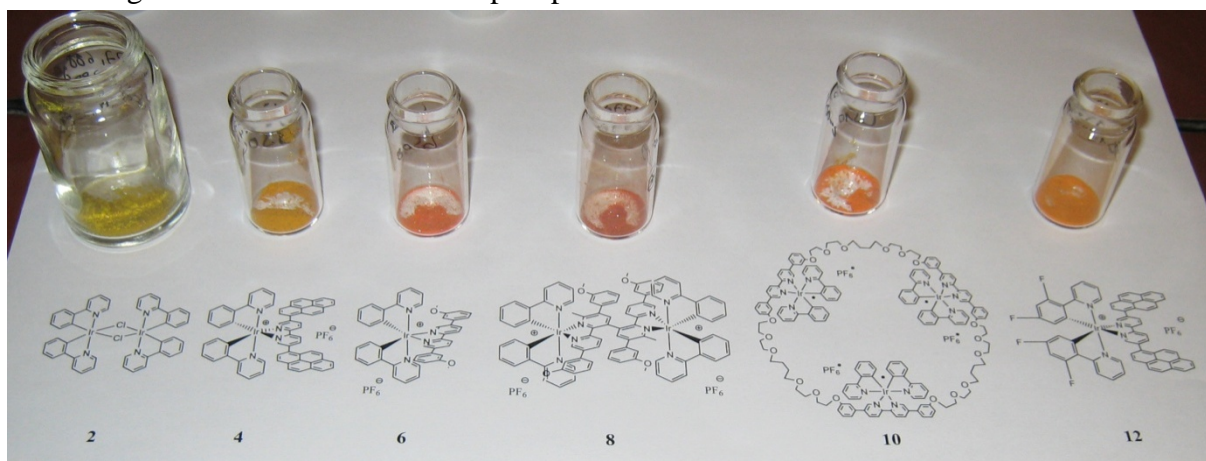

Figure 12: Photo of the synthesized iridium complexes.

In the following sections the syntheses and analyses of compounds **4** to **12** are described. The ^{1}H NMR spectra of compounds **4**, **6** and **12** are compared in a separate section.

4.1.1 Compound 4

Compound **2** and ligand **3** were dissolved in a mixture of methanol and dichloromethane and refluxed overnight. Since this did not result in the desired product, the microwave reactor was used for this reaction. After adding an excess of ammonium hexafluorophosphate, and filtration the residue was washed with

methanol. This work-up was done according to the procedure described by of *S. Graber*.

Crude compound **4** was used for crystal growing in dichloromethane layered with diethyl ether. The crystals obtained were only very small and some black precipitate was in the vial; this was probably unreacted pyrene ligand (compound **3**). After cleaning the product via column chromatography, the crystals obtained were bigger and were of X-ray quality.

The ESI-MS data are very clear with only the desired peak ($[M - PF_6]^+$) with the isotope pattern matching that simulated. For the elemental analysis, the calculated and the found values differ too much, but unfortunately calculations with additional molecules of solvent (dichloromethane, water, diethyl ether, methanol or ethanol) did not improve the result. The overall yield (72 %) is good despite the poor solubility of ligand 3.

The UV-Visible and the emission spectra of this compound were recorded prior to final purification. The latter showed two emission peaks after exciting at 360 nm. The second emission peak at 440 nm disappeared after column chromatography. After adding some free pyrene ligand **3** this peak was seen again. Therefore the spectra of the other compounds were measured only after chromatography.

4.1.2 Compound 6

Compound **6** was synthesized by dissolving compound **2** and ligand **5** in methanol and heating directly in the microwave reactor. In this reaction, dichloromethane was not used. The dichloromethane is needed to dissolve the ligand for the refluxing setup. In the microwave reactor with temperatures over 100 °C and pressures of about 14 bar there is no further need for dichloromethane. The reaction was done in pure methanol to be able to increase the temperature to 145 °C if needed.

Afterwards an excess of ammonium hexafluorophosphate was added and after filtration the residue was washed with water and diethyl ether to remove excess ammonium hexafluorophosphate. The crude solid was cleaned with a short column. In all the syntheses the column was needed to remove unreacted free ligand. Only one fraction was obtained.

Crystal growth needed some effort. The first crystals were of poor quality, yielding to a high R-factor of 15.95 %. After several attempts, the best crystals had a high, but much better, R-factor of 8.51 %. These crystals were grown from a solution of the complex dissolved in acetonitrile into which diethyl ether vapour diffused. The ESI-MS showed only the parent peak with the isotope pattern matching tha simulated. The elemental analysis agreed well with the calculated values.

4.1.3 Compound 8

Compound **2** and ligand **7** were dissolved in methanol and heated in the microwave reactor. In this reaction the colour change was quite dramatic from the green-yellow to a bright red. Ammonium hexafluorophosphate was not added directly to the mixture but firstly dissolved in distilled water. While adding this solution to the reaction mixture, the colour changed from red to pale orange. After filtration the residue was washed with water and diethyl ether.

Recrystallisation of the impure solid was unsuccessful, and therefore a short column was done. Afterwards the crude material was recrystallised from acetonitrile into which diethyl ether vapour diffused, but unfortunately there were no X-ray quality single crystals. The crystals were orange but were formed like thin plates and arranged like the spines of a hedgehog. Even after several weeks with different setups at room temperature and in the fridge, no single crystals could be grown and therefore no crystal structure could be determined.

The ESI-MS shows four peaks and all of them could be assigned (ESI, *m/z:* 501.1 [IrC$_{22}$N$_2$H$_{16}$] (calc. 500.59), 881.8 [M – 2PF$_6$]$^{2+}$ (calc. 882.04), 1262.9 [M – PF$_6$ – IrC$_{22}$N$_2$H$_{16}$] (calc. 1263.49), 1908.9 [M – PF$_6$]$^+$ (calc. 1909.04)). The elemental analysis has only small differences of 0.19 % and less between the calculated and found values.

Unfortunately the ^{1}H NMR spectrum looks like a forest (see Appendix)! There appears to be a mixture of complexes, most likely with one and two iridium atoms. Additionally the only symmetry in this compound **8** is an inversion centre resulting in many different protons, while the other compounds have higher symmetries. The spectrum of this compound can be seen in the Appendix. But from the results from the ESI and the elemental analysis it is clear that the synthesis worked well.

4.1.4 Compound 10

Ligand **9** was available as an oil with some impurities. To be able to transfer the ligand to the microwave vial it was dissolved in dichloromethane. This amount of dichloromethane was not removed for the heating in the microwave, because the earlier reactions worked well at temperatures about 110 °C. Dichloromethane can only be heated up to 110 °C in the microwave reactor. Compound 2 was added to the solution as well as methanol. After the heating the dichloromethane was evaporated and distilled water was added. This resulted in a colour change from orange to a milky white-orange.

An excess of ammonium hexafluorophosphate was added and after stirring for 1 hour the mixture was filtered. The residue was washed with water and diethyl ether yielding an orange solid. Not surprisingly, no crystals could be grown.

The ESI-MS shows several peaks which all could be assigned (ESI, *m/z:* 1070.9 [M – 3PF$_6$]$^{3+}$ (calc. 1071.27), 1355.8 [M – 2PF$_6$ – IrC$_{22}$N$_2$H$_{16}$]$^{2+}$ (calc. 1356.61), 1678.6 [M – 2PF$_6$]$^{2+}$ (calc. 1679.39).). These peaks show the existence of the ligand **9** coordinated to three iridium atoms and to only two iridium atoms. The element analysis is also quite good and again the ^{1}H NMR spectrum shows a forest of peaks. Only the CH$_2$-groups of ligand **9** could be seen with appropriate integrals. Figure 13 shows the integrals of one peak of compound **10**. The approximately
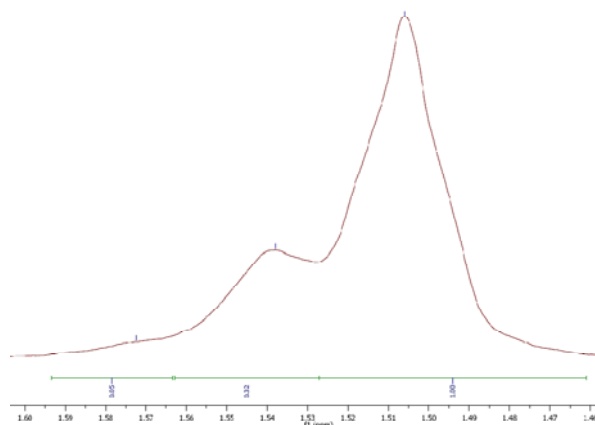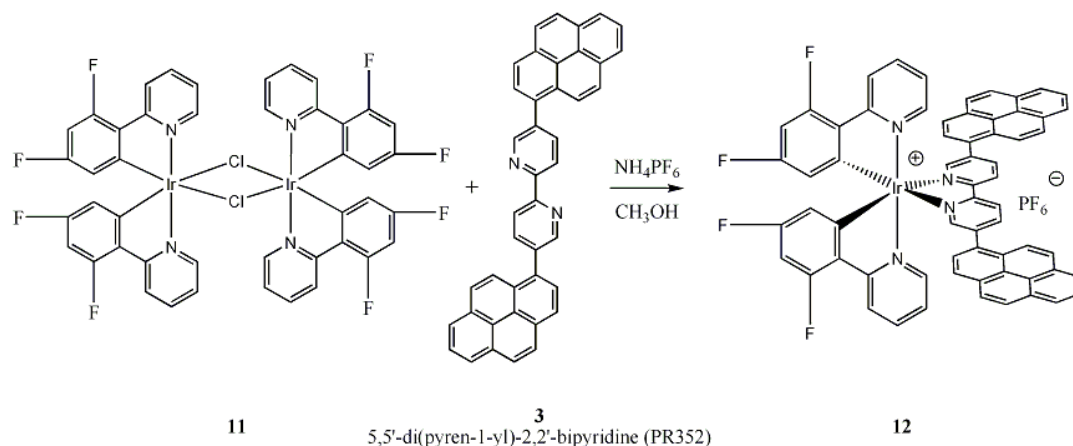

Figure 13: ^{1}H NMR peak of compound 10 to show the approximately ratio of LIr$_3$ to LIr$_2$ to LIr as 1.0 to 0.3 to 0.05.

18

ratio of LIr_3 to LIr_2 to LIr is 1.0 to 0.3 to 0.05. This can be estimated from the integrals from Figure 13. This fact increases the number of the remaining protons. The spectrum is shown in the Appendix with the integrals of the 6 CH_2-groups.

4.1.5 Compound 12

Scheme 2: Reaction scheme of compound 12.

In this work compound **12** is the only iridium complex with the fluorinated compound **11** as starting material instead of compound **2**. Similar to the synthesis of compound **4**, compound 11 was dissolved in methanol with ligand **3** and heated in the microwave reactor. After 1 hour there was still a black precipitate which was probably unreacted ligand **3**. Therefore the mixture was heated in the microwave reactor for further 30 minutes. During the heating period the pressure was very high (22 bar). After adding an excess of ammonium hexafluorophosphate the mixture was filtered and the residue was washed with water and diethyl ether yielding a green-yellow solid.

This solid was cleaned on a short column yielding a yellow solid. The crude solid was recrystallised from dichloroethane into which diethyl ether vapour diffused yielded and X-ray quality crystals. The R-factor for the structure determinate was only 2.56 %.

The ESI-MS is similar to compound **4** and contains only the desired peak ($[M - PF_6]^+$) with the isotope pattern matching that simulated.

4.1.6 ^{1}H NMR spectroscopic comparison

The ^{1}H NMR peaks of some of the synthesized complexes were at least partially comparable. A table of all complexes with the model complex (see Figure 14) from the PhD Thesis of *S. Graber* shows this effect. In Table 1 the shifts of the protons in ppm and the coupling constants in Hz are listed. The protons belong to the following phenyl and pyridine rings.

Rings A and B are both pyridine rings. There are clear trends for the proton signals in these two rings among the corresponding protons. The exact chemical shift is not significant but the arrangement of the peaks is constant. Another very helpful value is the coupling constant in Hz of these protons. It must be mentioned that only the model has a proton in the A5 position while the compounds **4, 6** and **12**
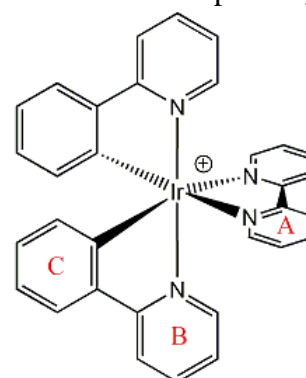
Figure 14: Scheme of the model (SG49) with the NMR labels in red.

have pyrene or phenyl rings in this position.

	A3		A4		A5		A6	
Model (SG **49**)	8.55	8.2 Hz	8.17	7.9 Hz	7.51	6.6 Hz	8.07	4.8 Hz
Compound **4**	9.25	8.4 Hz	8.69	8.3 Hz			8.19	1.8 Hz
Compound **6**	8.98	8.5 Hz	8.62	8.4 Hz			8.05	
Compound **12**	8.86	8.0 Hz	8.57	7.5 Hz			8.41	
	B3		B4		B5		B6	
Model (SG **49**)	8.01	8.2 Hz	7.83	7.8 Hz	7.04	6.6 Hz	7.54	5.6 Hz
Compound **4**	8.54	8.2 Hz	8.11	7.8 Hz	7.32	6.6 Hz	8.17	4.9 Hz
Compound **6**	8.29	8.2 Hz	7.94	7.8 Hz	7.17	6.6 Hz	7.85	5.7 Hz
Compound **12**	8.54	8.7 Hz	8.01	8.0 Hz	7.24	6.4 Hz	7.91	5.6 Hz
	C3		C4		C5		C6	
Model (SG **49**)	6.36	7.6 Hz	6.98	7.4 Hz	7.12	7.5 Hz	7.79	7.8 Hz
Compound **4**	6.28	7.4 Hz	6.69	7.3 Hz	6.74	7.4 Hz	7.98	7.7 Hz
Compound **6**	6.33	7.5 Hz	6.97	7.5 Hz	7.07	7.5 Hz	7.98	7.8 Hz
Compound **12**			5.80	8.2 Hz			6.38	10.7 Hz

Table 1: Comparison of the ^{1}H NMR spectra (δ/ppm) and the coupling constants [Hz] of compounds 4, 6 and 12.

The influence of the two fluorine atoms of compound **12** on the ring C in position 3 and 5 are clearly visible in the completely different shifts and coupling constants of the two protons in position 4 and 6.

4.2 Crystal structures

The crystals in this work were grown in the following setups. The first trial was always the recrystallisation from dichloromethane layered with diethyl ether. The next trials were done the following way: the complexes were dissolved either in dichloromethane, dichloroethane or acetonitrile and put in an atmosphere of either diethyl ether or ethyl acetate vapour. The effect of the latter two solvents is to lower the solubility of the complex and therefore start the slow precipitation of the complexes. If the right setup was found, X-ray quality crystals grew slowly. The crystals were grown at room temperature (about 298 K) or in the fridge (278 K).

X-ray quality crystals of compound **4** were grown and the structure could be resolved with an R-factor of 4.38 %. Compound **6** needed more attempts to finally get the structure with a high R-factor of 8.51 %.

Well-formed single crystals of the most interesting compound **12** were grown resulting in a structure with an excellent R-factor of only 2.56 %.

4.2.1 Comparison of compounds 4 and 12

In Table 2 distances between the metal centre (Ir1) and the six directly bonded atoms are listed. N1 and N2 belong to the pyrene ligand where N3 and C53, and N4 and C64 belong to the two phenyl pyridines.

Compound 4		Length [Å]
Ir1	N1	2.136(4)
Ir1	N2	2.131(2)
Ir1	N3	2.045(4)
Ir1	C53	2.026(4)
Ir1	N4	2.053(4)
Ir1	C64	2.013(3)

Compound 12		Length [Å]
Ir1	N1	2.133(2)
Ir1	N2	2.124(2)
Ir1	N3	2.038(3)
Ir1	C53	1.998(3)
Ir1	N4	2.033(3)
Ir1	C64	2.002(2)

Table 2: Comparison of the distances around the iridium centre of compound 4 (left) and compound 12 (right) in Angstrom units.

Figure 15: compound 12 shows no intra molecular π-stacking. shows the structure of compound **12**. There is no intramolecular π-stacking between the aromatic rings. Compound **12** is shown with the counterion [PF$_6$]$^-$. The two pyrene groups are each planar and twisted at an angle of 72.02° with respect to the pyridine rings to which they are attached.
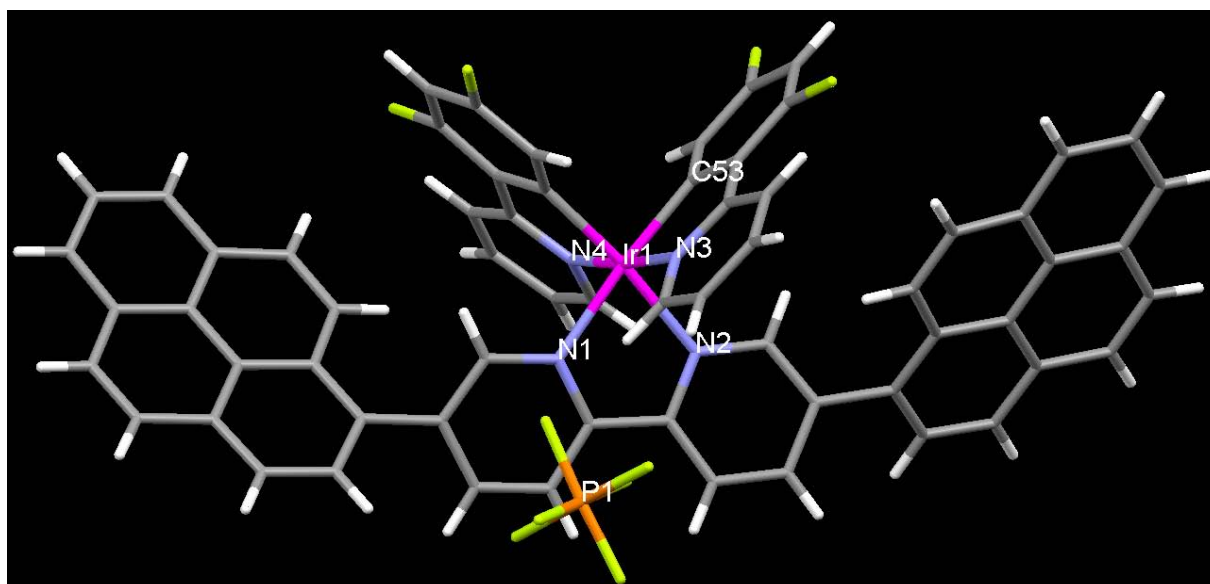

Figure 15: compound 12 shows no intra molecular π-stacking.

The distances in the two complexes are very similar with differences of only about 0.02 Å. The influence of the fluorine atoms on these distances around the metal centre is therefore not very strong.

The crystal structure of compound **12** shows dimer formation via π-stacking of the pyrene groups with a distance of 3.6 Å between the planes of the stacked pyrene groups. This separation is similar to that found in graphite. The dimers are shown in Figure 16 without their counterions. The pyrene groups of only two molecules interact, so no polymer formation occurs.

The next interaction of the dimer forming molecules concerns the fluorinated phenyl rings around the iridium(III) centre. The edge – to – face interactions between the hydrogen at position 4 in the phenyl ring and two other fluorinated phenyl rings of another molecule is about 2.6 Å while the two fluorinated phenyl rings have also π-stacking at a distance of 3.4 Å. These close contacts are shown in Figure 17.
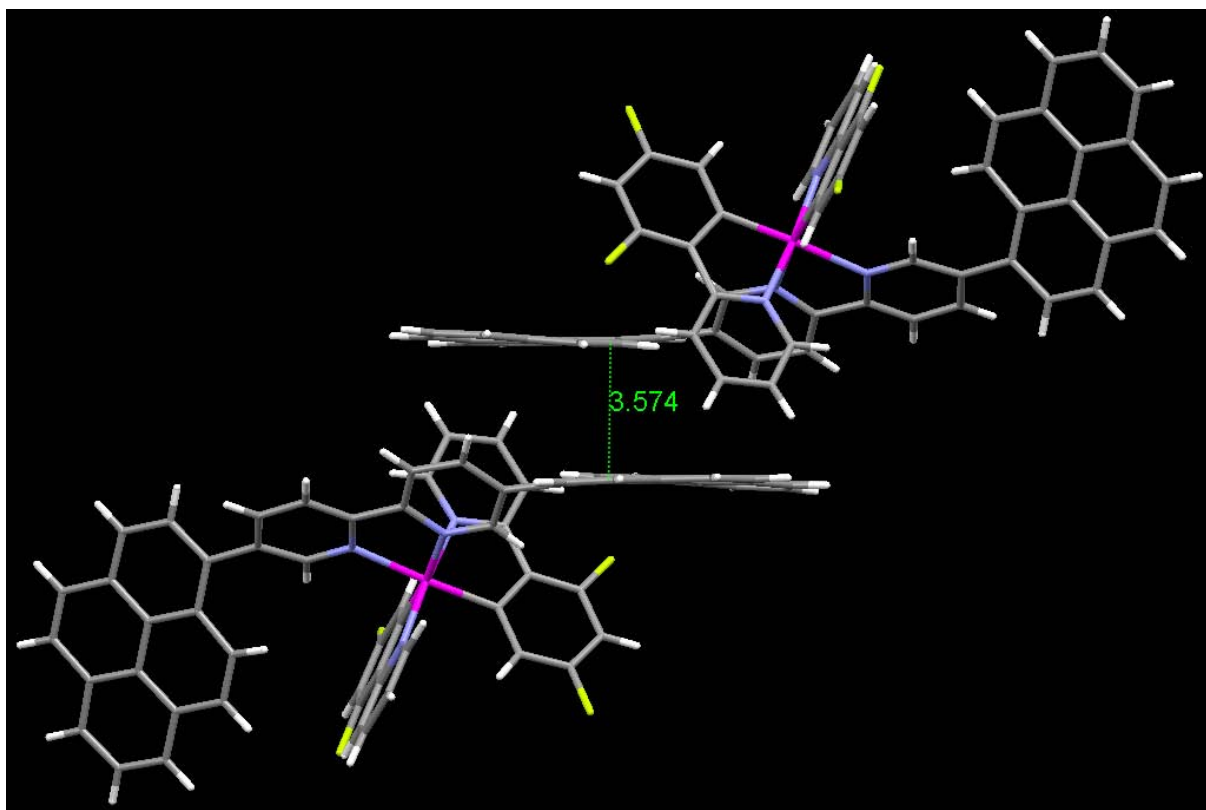
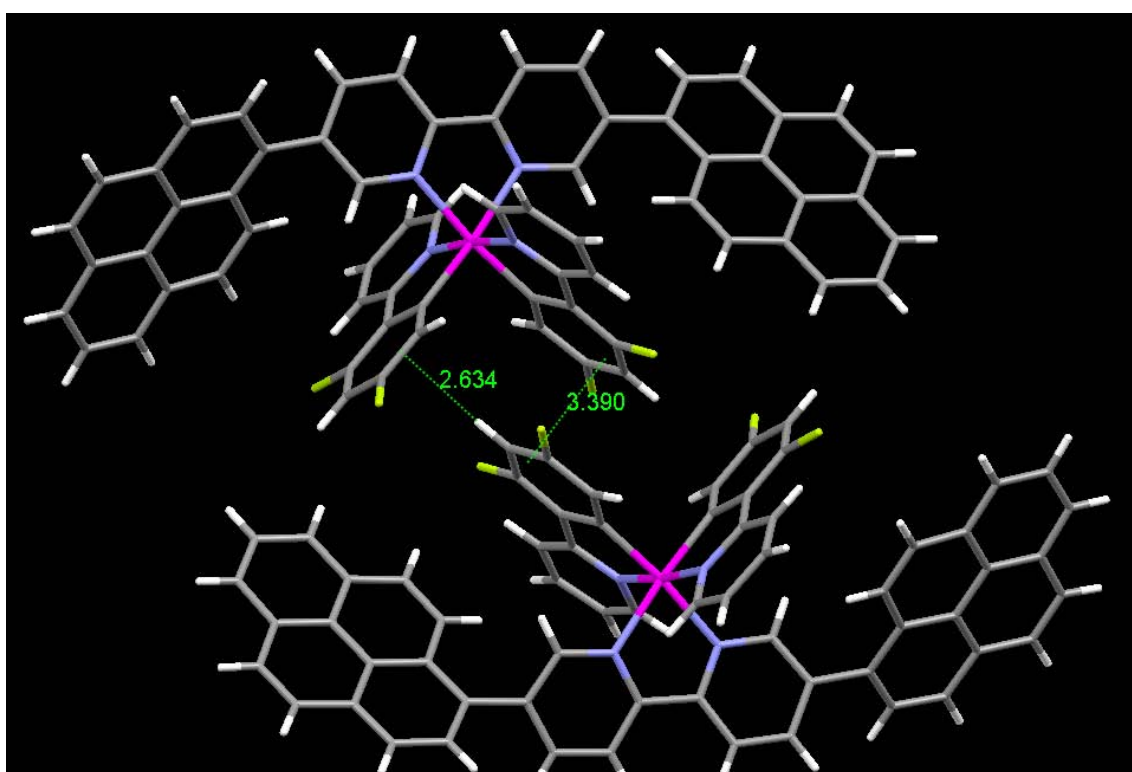**Figure 16: Dimers of compound 12 through π -stacking of the pyrene groups.**

Figure 17: Close contacts between the fluorinated phenyl rings of compound 12

The arrangement of the pyrene groups of some molecules of compound **12** are shown in Figure 18. With this viewing angle it is obvious that the pyrene groups are all well aligned with the angle of 72.02° in between.

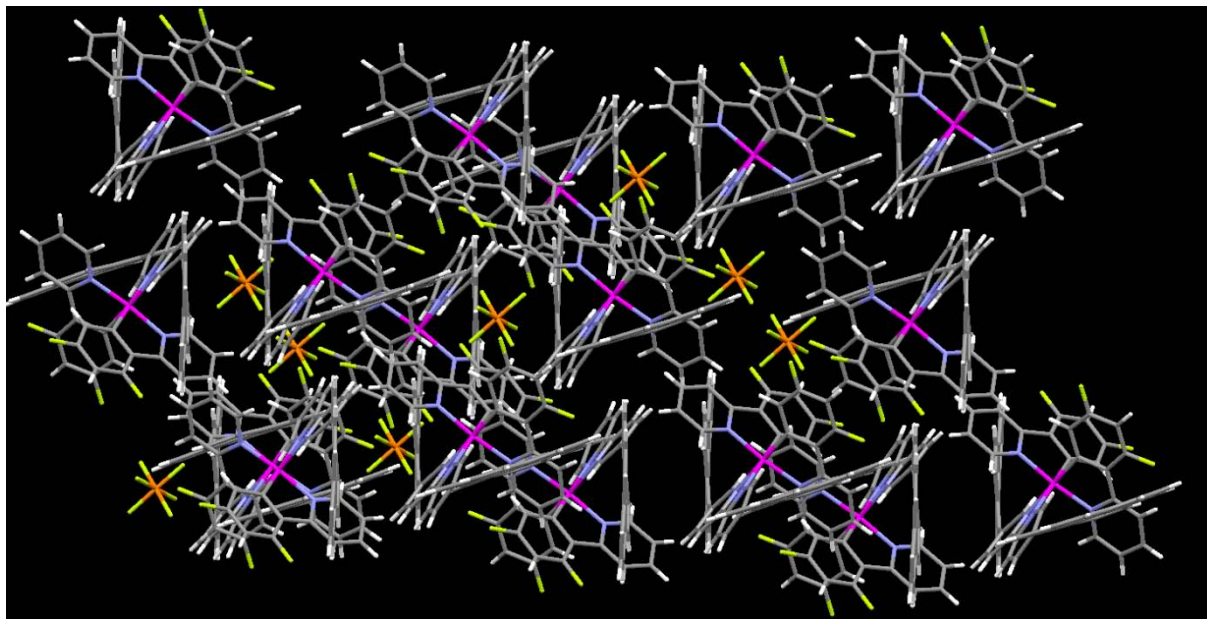**Figure 18: Focus on the well arranged pyrene groups with an intra molecular twisting angle of 72.02°.**

The non-fluorinated compound **4** shows also the pyrene dimers like compound **12**. As can be seen in Figure 19 the spatial arrangement of the dimers is completely different. The distance between the pyrenes is slightly closer with 3.5 Å.

The twisting angle within a pyrene ligand is bigger with 88.07°. But there is no π-stacking between the phenyl groups.

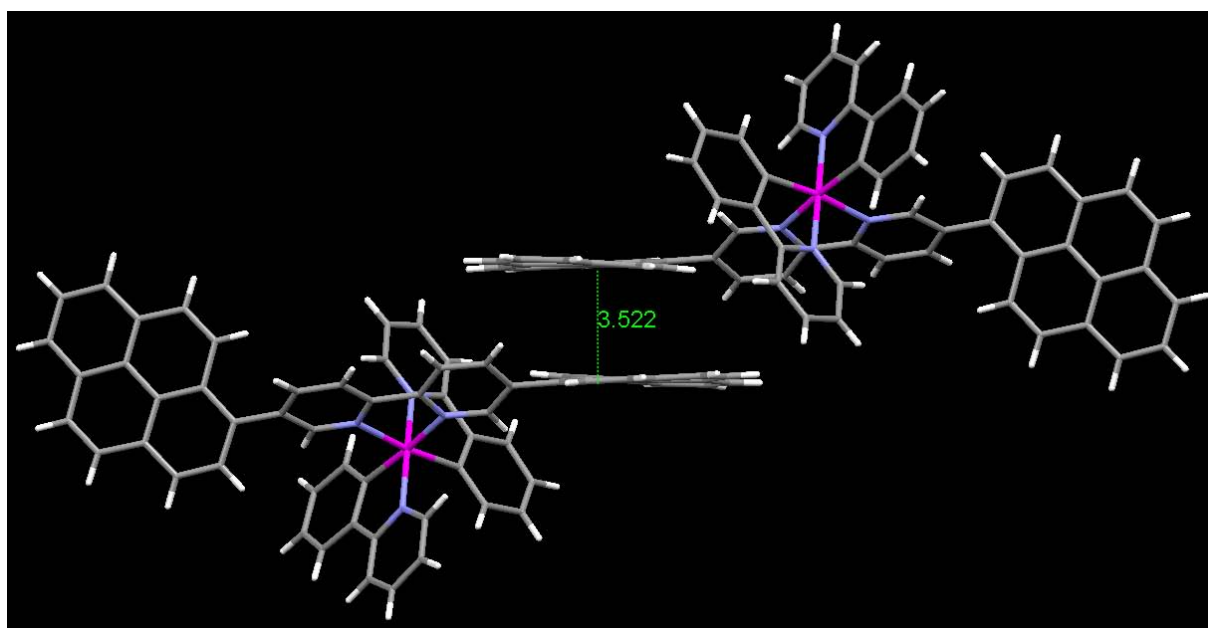**Figure 19: Dimer formation of compound 4 with a distance of 3.5 Å between the pyrene groups.**

4.2.2   Compound 6

The crystal structure of compound **6** also shows no intramolecular π – stacking, as can be seen in Abbildung 20. The following Table 3 shows that ligand **5** of compound **6** is about 0.01 Å further away than the ligand **3** of compound **12**, but this probably within the experimental error. As a result the distances of the phenyl pyridines are also slightly different.

Compound 6		Length
Ir1	N1A	2.142(8)
Ir1	N2A	2.143(7)
Ir1	N3A	2.038(8)
Ir1	C25A	2.00(1)
Ir1	N4A	2.063(8)
Ir1	C36A	2.014(9)

Compound 12		Length
Ir1	N1	2.133(2)
Ir1	N2	2.124(2)
Ir1	N3	2.038(3)
Ir1	C53	1.998(3)
Ir1	N4	2.033(3)
Ir1	C64	2.002(2)

Table 3: Distances around the iridium centre of compound 6 (left) and compound 12 (right).

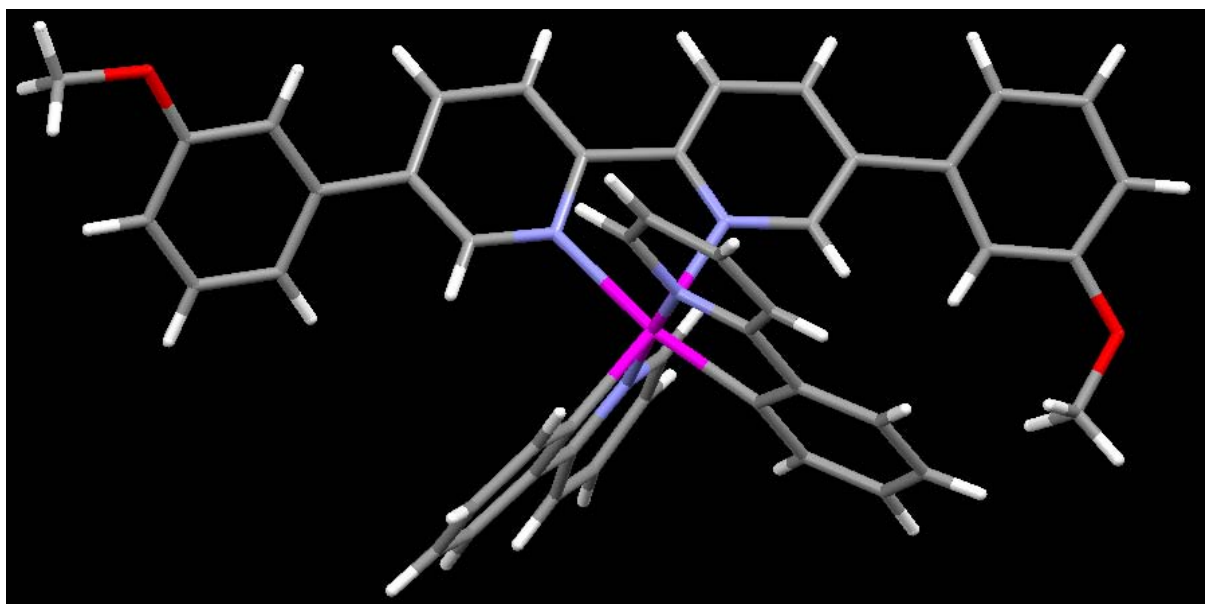The twisting angle between the two phenyl rings of the ligand is 66.10°.

Abbildung 20: Crystal structure of compound 6 shows no intra molecular π – stacking.

Unlike the crystal structures of the compounds **4** and **12**, compound **6** does not show any intermolecular π – stacking. But as shown in Figure 21, the phenyl groups of the ligand of two different molecules of compound **6** are at a distance of only 3.9 Å. The planes of the two phenyl rings are not parallel. The angle between the two phenyl rings is 13.9°. The crystal structure is with an R-factor of 8.51 % not as good as the structures of compounds **4** and **12** and therefore the errors of the bond lengths and angles in this structure are larger.
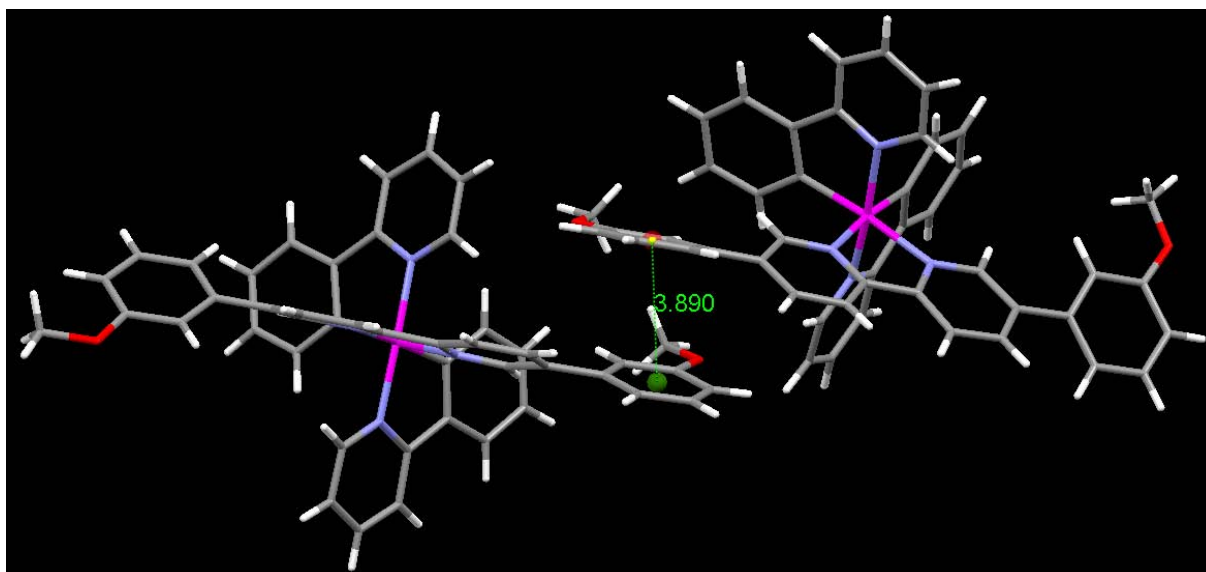
Figure 21: Very close interaction of two molecules of compound 6.

4.3 UV-Visible spectroscopic measurements

Since all the complexes in this work were produced for photonic applications the UV-Visible spectra of all the compounds were recorded. UV-Visible measurements are absorption spectra covering the ultra violet range (UV, about 200 nm) through to 900 nm. The visible range is from violet at 400 nm up to red at 800 nm. To be mentioned that the visible colour is not equal to the absorbed colour.

From these spectra the wavelengths where the compound can be excited for the emission can be determined. For all the absorption and luminescence measurements the compounds were dissolved in pure dichloromethane at concentrations of $1.0*10^{-5}$ and $1.0*10^{-6}$ M. In the following figures the measurements are for solutions of $1.0*10^{-5}$ M concentrations.

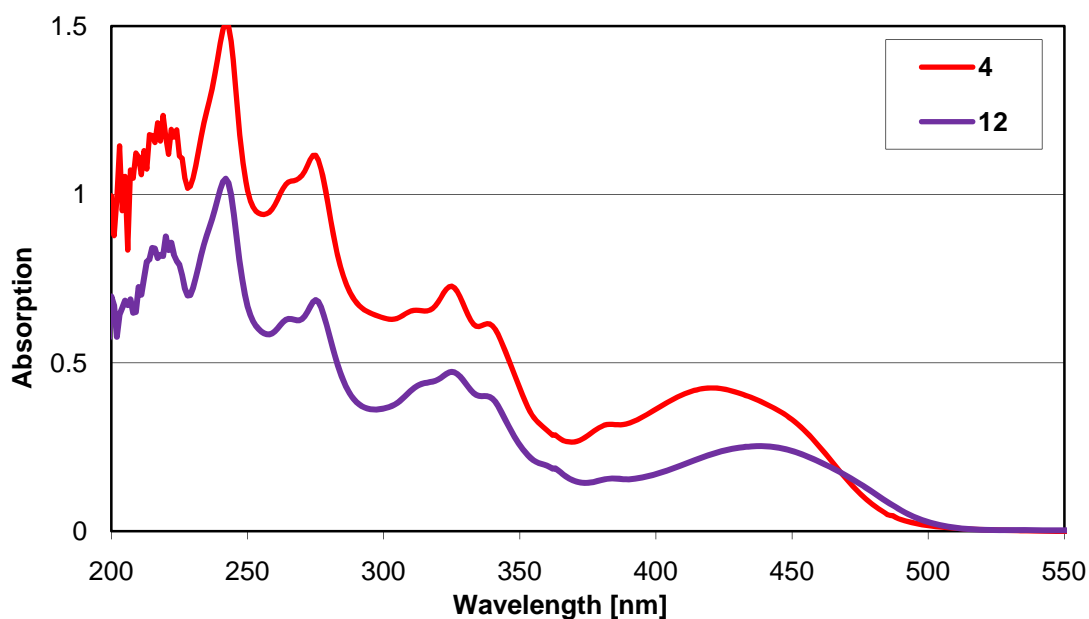**Figure 22: UV-Vis absorption of compounds 4 and 12 at $1.0*10^{-5}$ M**

In Figure 22 the absorption spectra of compound **4** (in red) and compound **12** (in violet) are drawn. These two curves are very similar with only small differences in the range around 430 nm. Unlike the other three compounds **6**, **8** and **10** they have this peak in the visible range. The UV-Vis spectra of the three compounds **6**, **8** and **10** are shown in Figure 24. These three spectra are also comparable. The main difference between the spectra of compounds **4** and **12** and compounds **6**, **8** and **10** is the additional absorption maximum at 420 nm and 439 nm of compound **4** and compound **12**, respectively, and this arises from the pyrene ligand.
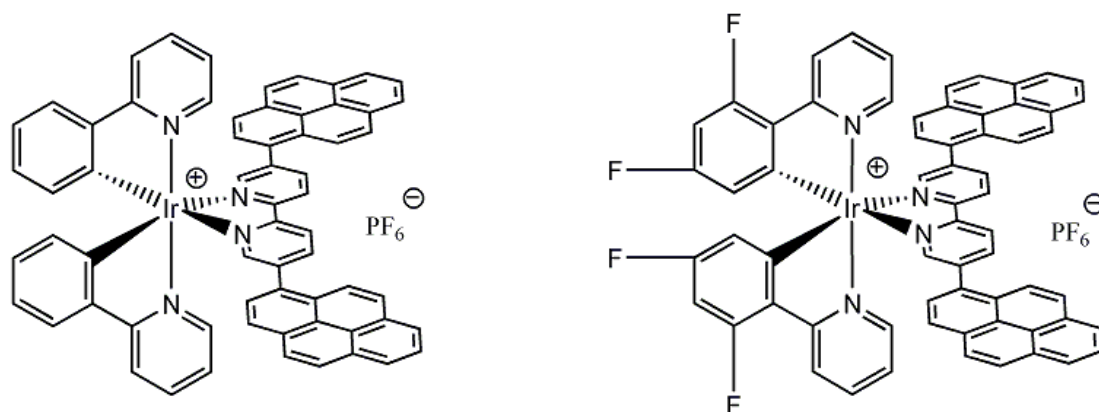

Figure 23: Structures of compounds 4 (left) and 12 (right).

This additional peak in compound **4** and **12** is due to *metal-to-ligand charge transfer* (MLCT). MLCT means a transfer of an electron from an orbital with primarily metal character to an orbital with primarily ligand character. These two complexes have the same pyrene ligand (**3**) and the only differences are the four fluorine atoms replacing the hydrogen atoms at positions 4 and 6 of the two phenyl rings which are linked to the pyridines. The differences can be seen in Figure 23.

Due to this change from hydrogen to fluorine, the broad absorption peak around 430 nm is slightly shifted. The hydrogenated compound **4** has the maximum at 420 nm while the fluorinated compound **12** has the maximum at 440 nm. A shift to longer wavelengths (λ) is a reduction of the energy, as seen in the following equation.

$$E = h * v = h * c / \lambda$$

h: Planck constant, v: frequency, c: speed of light, λ: wavelength

Incorporating fluorine atoms into the ligand should lower the level of the lowest unoccupied molecular orbital (LUMO).

The three compounds **6**, **8** and **10** have also very similar absorption curves due to the fact that they contain comparable ligands. The structures of the three compounds are shown in Figure 25. The environment of the iridium(III) centres are very similar in all three compounds. Bound to the bipyridine are two phenyl rings with a methoxy group. The absorption spectra of these three compounds in Figure 24 look very similar.
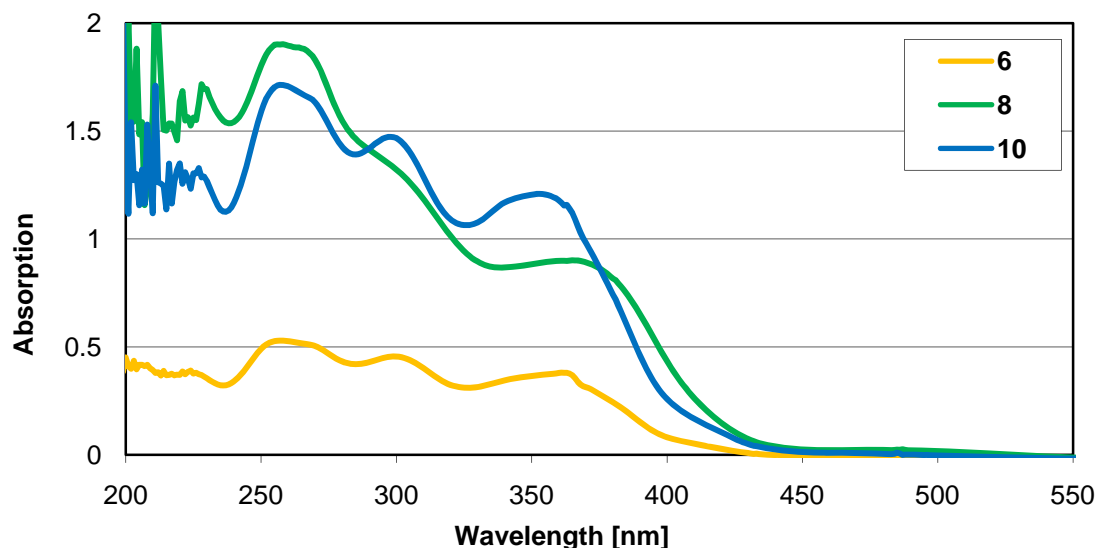
Figure 24: UV-Vis absorption of compounds 6, 8 and 10

The peaks in the UV range are due to ligand-centred $\pi^* \leftarrow \pi$ transitions. This means an electron is transferred from an occupied and bonding π orbital to an antibonding π^* orbital.
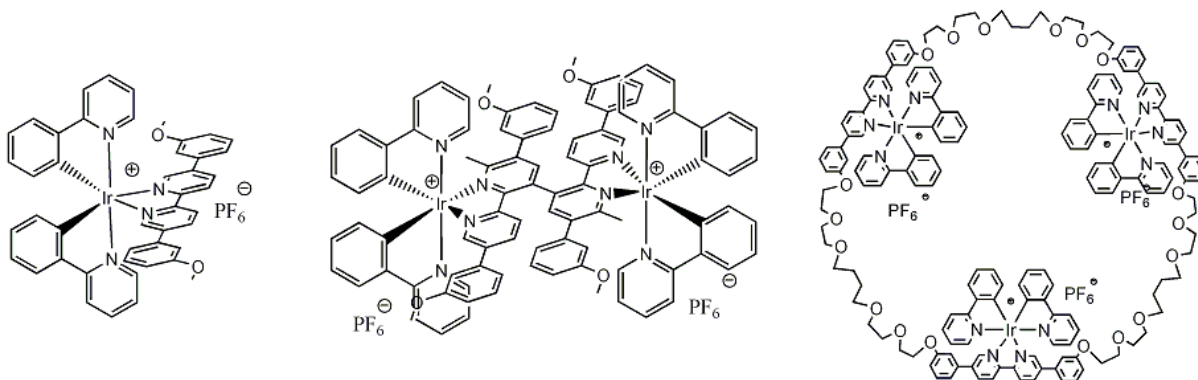

Figure 25: Structures of compounds 6 (left), 8 (centre) and 10 (right).

4.4 Electroluminescence measurements

Following the absorption measurements emission spectra were recorded for all of the iridium complexes. These were dissolved in dichloromethane at a concentration of $1.0*10^{-5}$ M. In the following Figure 26 the graphs of the emissions of the three comparable compounds **6**, **8** and **10** resulting from an excitation around 360 nm are shown.

Again, the three compounds **6**, **8** and **10** show very similar spectra with a main emission around 600 nm, which is characteristic of the emission of many iridium complexes (see PhD of *S. Graber*). Emissions at 600 nm result in an emitted orange colour. It should be mentioned that the small, sharp peaks at around 700 nm are upper harmonic oscillations of the excited wavelength.
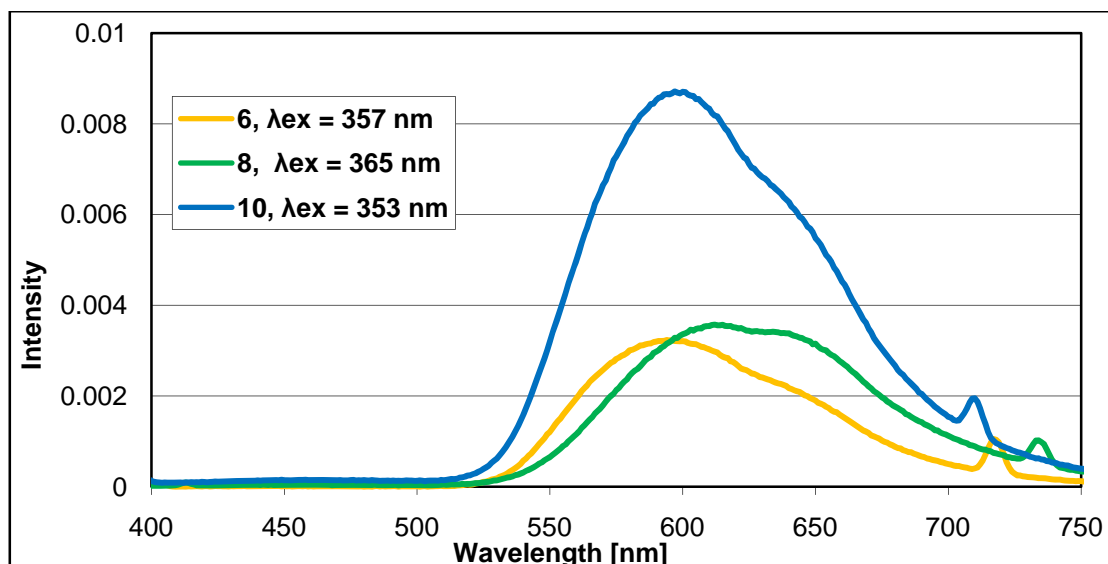
Figure 26: Emission spectra of compounds 6, 8 and 10 in dichloromethane at a concentration of 1.0*10-5 M, excited at the noted wavelengths with the emission and excitation slits at position 3.

Shown in Figure 27 are the emission curves of the two pyrene compounds **4** and **12**. The curve of compound **4** (in red, excited at 350 nm) interestingly shows no characteristic emission at 600 nm, but a "new" emission maximum at 450 nm. Comparison with the emission spectrum of the free pyrene ligand of *P. Rösel* shows the maximum at 447 nm. Compound **4** shows emission of the pyrene groups and no iridium emission. This complex was designed to have two simultaneous emissions, one from the iridium centre and a second from the pyrene groups. Unfortunately this was not observed.
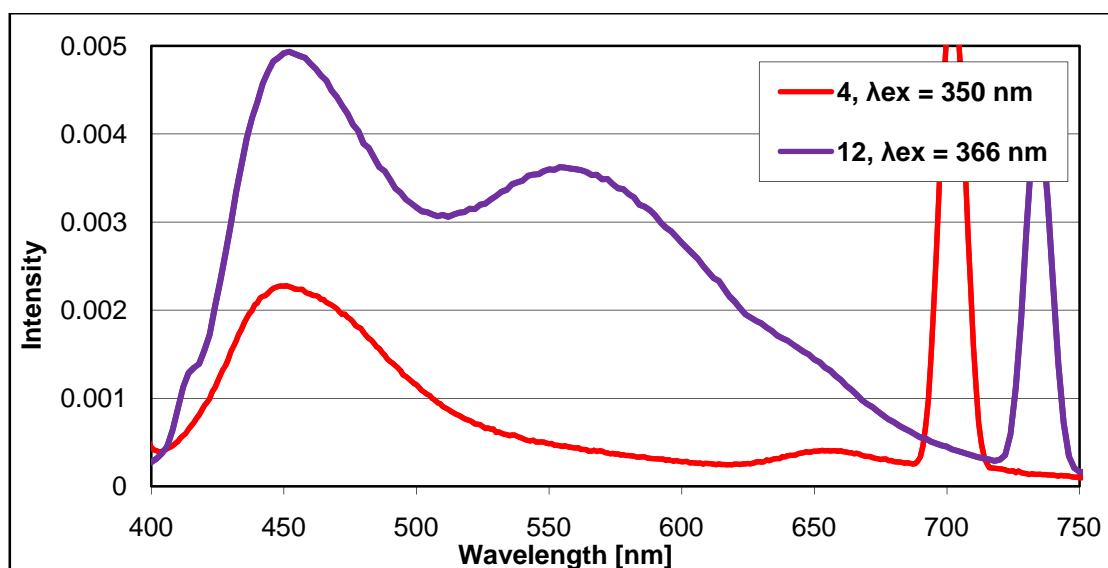
Figure 27: Emission spectra of compounds 4 and 12 complexes in dichloromethane in a concentration of 1.0*10^{-5} M, excited at the noted wavelengths with the emission and excitation slits at position 5.

The most interesting behaviour was shown by the fluorinated compound **12**, drawn in violet in the Figure 27. The measurements were repeated over several days and with different excitation wavelengths but the results are the same: the curve shows two

peaks, meaning it is a dual emitter. The two emission maxima are at 450 and 556 nm. Again the 450 nm emission is from the pyrene ligand and the emission at 556 nm must come from the iridium metal centre. The wavelength is blue-shifted about 50 nm compared to the "normal iridium emission" of 600 nm.

Figure 28: Photo of the emission of compound 12 from excitation at 350 nm.

The emission of compound **12** dissolved in dichloromethane can be seen in Figure 28. The blue-white colour is from the excitation at 350 nm with fully opened slits.

It is also very interesting that the emission spectrum of compound **12**, freshly dissolved in dichloromethane changes significantly over a period of a few hours as seen in Figure 29.
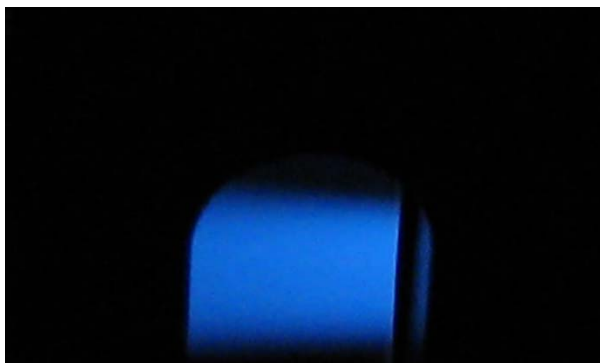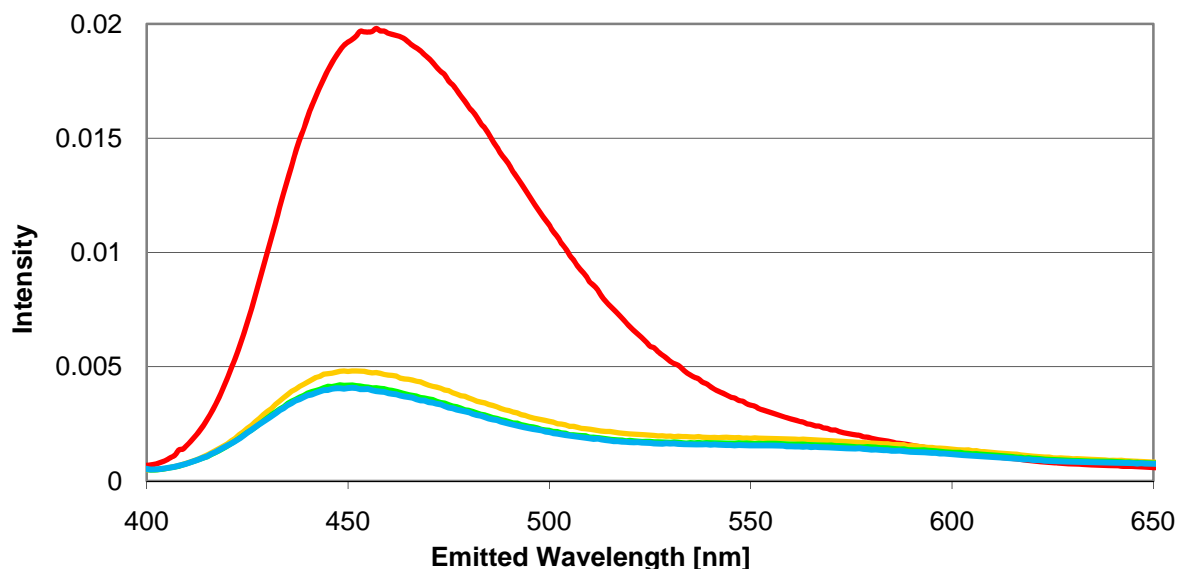

Figure 29: Emission spectra over the time of compound 12 freshly dissolved in dichloromethane at a concentration of $1.0*10^{-5}$ M, excited at 350 nm, emission and excitation slits 5.

Just after dissolving the compound in dichloromethane, the first emission spectrum shows only the pyrene peak at 450 nm, but a very high intensity. Over time, this peak decreases in intensity and the iridium peak at 550 nm appears. It is also possible that the iridium peak is also present at the beginning with low intensity but not seen in comparison with the big pyrene peak. The origin of this behaviour is still unclear.

4.5 Excitation Measurements

Excitation measurements of all five complexes were also recorded. They confirmed in all cases the corresponding absorption spectrum. Only the excitation spectrum of the dual emitter will be discussed here. The curves in Figure 30 show that the emission at 450 nm is excited at 357 nm while the emission at 550 nm results from the excitation at 350 and 440 nm.
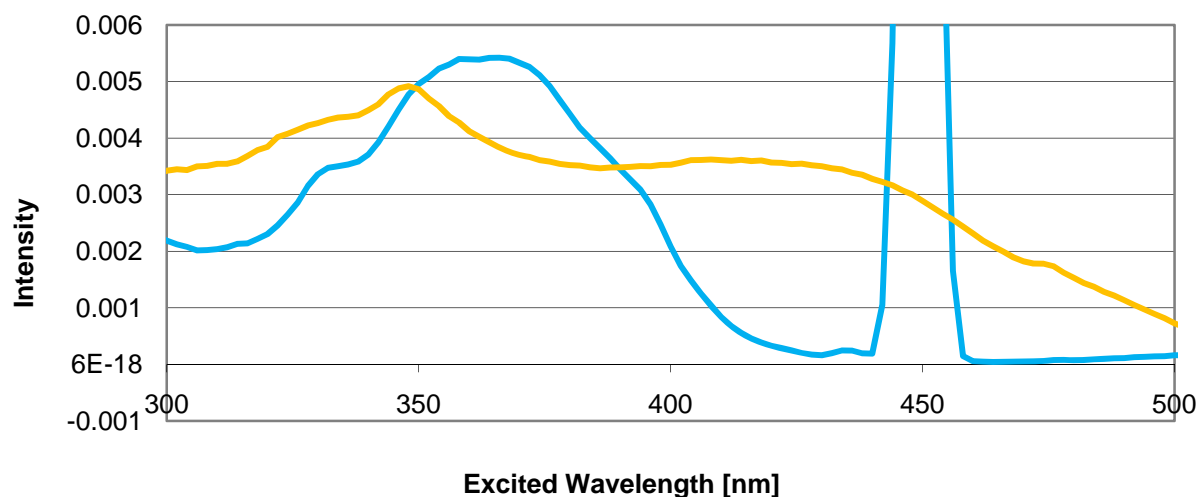
Figure 30: Excitation spectrum of compound 12 in dichloromethane at a concentration of 1.0*10⁻⁵ M for the emissions at 450 nm and 556 nm.

4.6 Lifetime, Quantum Yield and Square Wave measurements

With compound 12 further measurements were carried out. The lifetime was determined as $\tau = 374 \; ns$. The quantum yield in aerated dichloromethane solution was calculated with the following equation.[9]

$$\phi(sample) = \phi(ref.) * \frac{Abs(ref.) * n(sample)^2 * I(sample)}{Abs(sample) * n(ref.)^2 * I(ref.)}$$

Abs = absorption, n = index of refraction of the solvent, I = intensity of the emission. $n_{DCM} = 1.4242$ and $n_{MeCN} = 1.3442$.

The measurements were carried out at 350 nm and resulted in

$$\phi(compound \; \mathbf{12}) = 0.028$$

This value is relatively low compared with the iridium complexes synthesised by *S. Graber*, but it must be mentioned that no optimization of the solvent has been carried out so far in this work.

Electrochemistry measurements were also performed. 5 mg of compound **12** was used in the setup described in chapter 2. Due to the poor solubility of the compound in acetonitrile, not all of the 5 mg dissolved and the cyclic voltammetry showed no specific peaks. Therefore the values were measured via square wave yielding the following values, each value versus the internal standard ferrocene.

$Ir^{3+/4+}$: +0.976 V and three more peaks from the reduction of the ligand: -0.817 V, -1.059 V, -1.398 V.

As mentioned in Chapter 3, 50 mg of compound 12 were sent to Spain to the group of *Dr. Henk Bolink*. The compound will be tested in LEECs and in OLEDs, but so far they have no verified results.
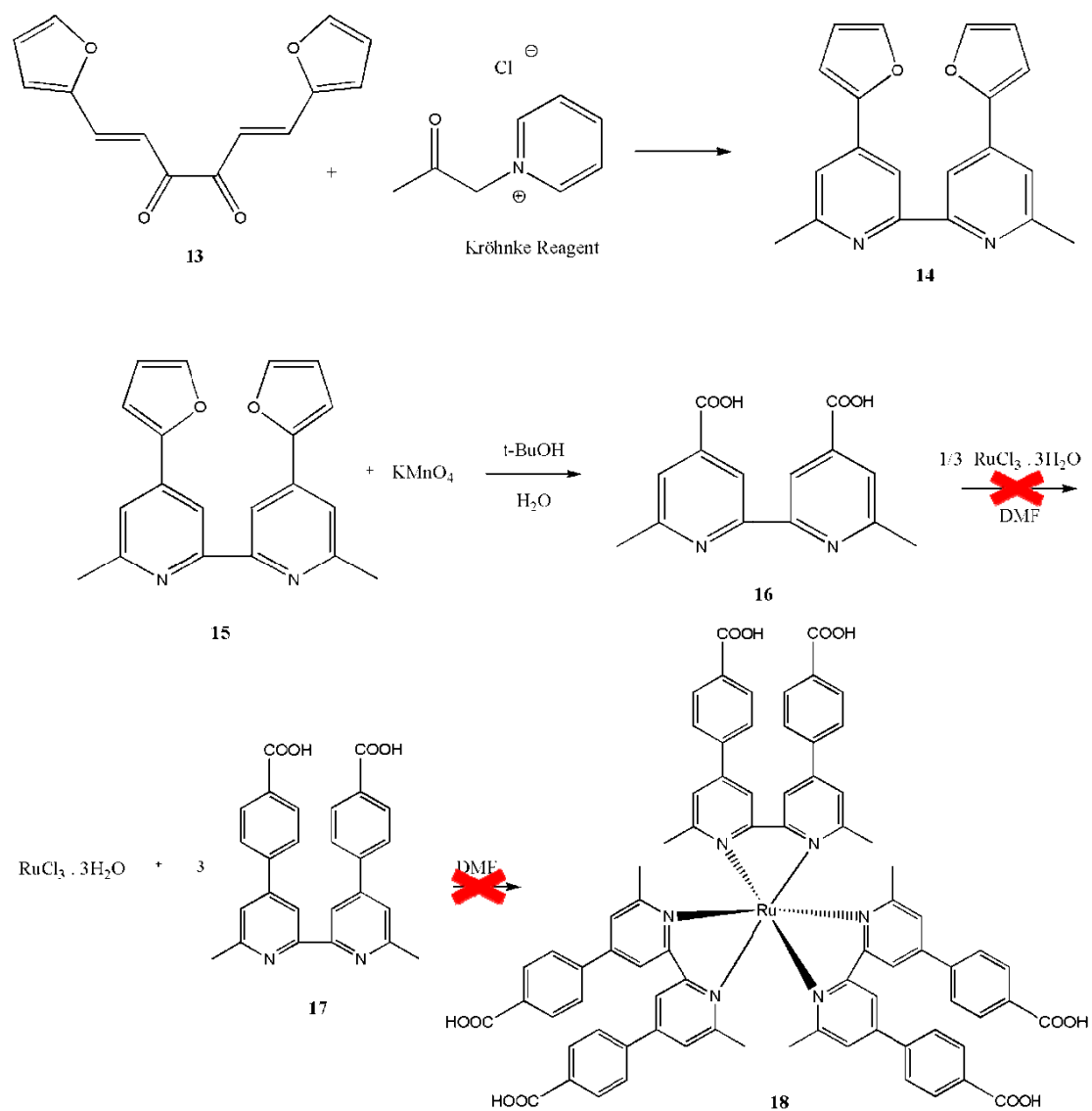
4.7 Ruthenium complexes

The most time consuming activity during this work was the synthesis of the ruthenium complexes. The motivation for making these complexes was to exchange the non fluorescent $[PF_6]^-$ anion for a fluorescent ruthenium complex as counter ion. The $[PF_6]^-$ anion has a negative charge. Ruthenium usually has a charge of +2 or +3. To be able to use the ruthenium complex as a counterion, carboxylic acid-substituted bipyridines were used. After deprotonation of these acid groups, the ruthenium complex will have a negative charge and should therefore act as an anion for the iridium complexes.

The main problem with this approach is probably the different band gaps of the two metal centres iridium and ruthenium. In a 1:1 ratio the excited electrons of the iridium will probably migrate to the ruthenium, due to the lower energy level of the LUMO of the latter. In this setup only a ruthenium emission will be seen.

The synthetic route used to prepare the ruthenium complex is shown in Scheme 3. However, this complexation did not work, and we attributed the failure to the presence of the 6- and 6'-methyl groups.

The next approach is shown in Scheme 4. Starting from 4,4´-dimethylbipyridine, we attempted to prepare the target complex **23** with 4,4´-dicarboxylicacid-bipyridines. This complexation was attempted with the diacid bipyridine and the esterified bipyridine. The esterification was done in order to clean the product on a column. Unfortunately the whole synthesis consumed too much time to be able to finish this trial within the time constraints of the master work. Instead, the remaining time was used to fully characterise the new and very interesting compound **12**.[19-26],[28],[30-34]

Scheme 3: Syntheses towards ruthenium compound 18. The red crosses indicate the unsuccessful complexation reactions.
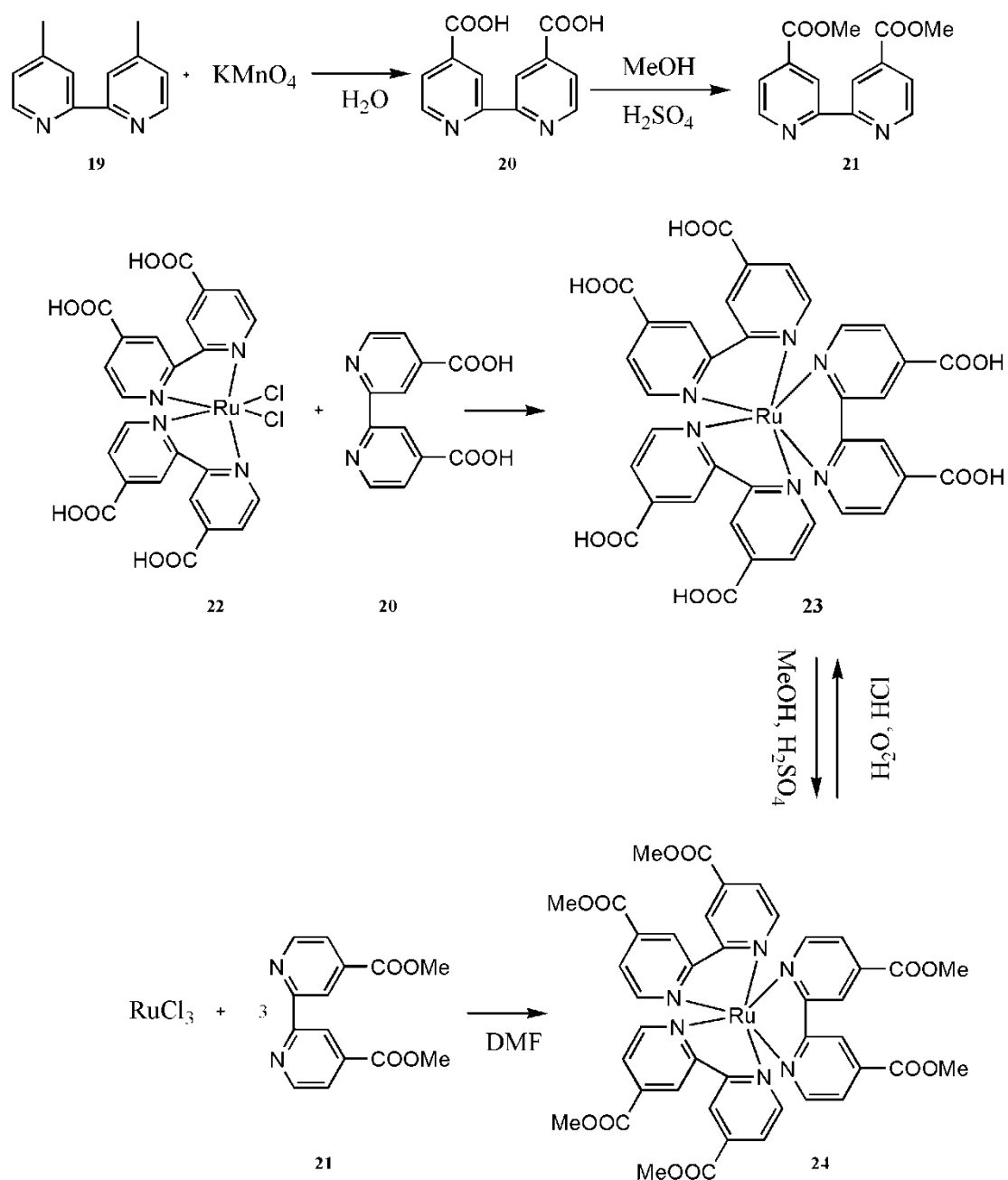
Scheme 4: Syntheses towards ruthenium compound 23.

5. Acknowledgements

6. References

[1]   H. J. Bolink, E. Coronado, R. D. Costa, E. Ortí, M. Sessolo, S. Graber, K. Doyle, M. Neuburger, C. E. Housecroft, E. C. Constable, *Adv. Mater.*, **2008**, 20, 1 - 4

[2]   K. A. King, R. J. Watts, *J. Am. Chem. Soc.*, **1987**, 109, 1589 – 1590

[3]   S. Sprouse, K. A. King, P. J. Spellane, R. J. Watts, *J. Am. Chem. Soc.*, **1984**, 106, 6647 – 6653

[4]   S. Graber, PhD Thesis, University of Basel, **2009**

[5]   C. E. Housecroft, A. G. Sharpe, Inorganic Chemistry, Prentice Hall, **2007**, 3rd Edition.

[6]   C. Mortimer, U. Müller, Chemie, Thieme, **2003**, 8th Edition.

[7]   URL: www.chemie.unibas.ch/~constable as of July 2009

[8]   G. Schneider, Report of the second project work, **2009**

[9]   P. Rösel, PhD Thesis, University of Basel, **2009**

[10]   P. Tipler, G. Mosca, Physik für Wissenschaftler und Ingenieure, Elsevier, **2004**, 2nd Edition.

[11]   URL: www.wikipedia.org as of July 2009

[12]   Stoe & Cie, IPDS software v 1.26, Stoe & Cie, Darmstadt, Germany, 1996.

[13]   G. M. Sheldrick, *Acta Crystallogr., Sect. A* **2008**, *64*, 112-122.

[14]   COLLECT Software, Nonius BV 1997-2001.

[15]   A. Altomare, G. Cascarano, G. Giacovazzo, A. Guagliardi, M. C. Burla, G. Polidori, M. Camalli, *J. Appl. Cryst.* **1994**, *27*, 435-435.

[16]   Z. Otwinowski, W. Minor, *Methods in Enzymology*, vol. 276, ed. by C.W. Carter, Jr and R.M. Sweet, **1997**, Academic Press, New York, pp. 307.

[17]   P. W. Betteridge, J. R. Carruthers, R. I. Cooper, K. Prout, D. J. Watkin, *J. Appl. Cryst.* **2003**, *36*, 1487-1487.

[18]   I. J. Bruno, J. C. Cole, P. R. Edgington, M. K. Kessler, C. F. Macrae, P. McCabe, J. Pearson, R. Taylor, *Acta Crystallogr., Sect. B*, **2002**, **58**, 389-397.

[19]   K. Kalyanasundaram, Md. K. Nazeeruddin, M. Graetzel, *Inorg. Chim. Acta,* **1992**, 198-200, 831-839.

[20]   F. H. Case, *J. Am. Chem. Soc.,* **1946**, 68, 2574.

[21]   H. Xia, Y. Zhu, D. Lu, M. Li, C. Zhang, B. Yang, Y. Ma, *J. Phys. Chem. B.,* **2006**, 110, 18718-18723.

[22]   A. F. Morales, G. Accorsi, N. Armaroli, F. Barigelletti, S. J. A. Pope, M. D. Ward, *Inorg. Chem.,* **2002**, *41*, 6711-6719.

[23]   S. Anderson, E. C. Constable, K. R. Seddon, J. E. Turp, J. E. Baggott, M. J. Pilling, *J. Chem. Soc. Dalton Trans.,* **1985**, 2247-2261.

[24]   A. Yoshimura, Md. J. Uddin, N. Amasaki, T. Ohno, *J. Phys. Chem. A,* **2001**, *105*, 10846-10853.

[25]   A. Guerrero-Martínez, Y. Vida, D. Domínguez-Gutiérrez, R. Q. Albuquerque, L. De Cola, *Inorg. Chem.,* **2008**, *41*, 9131-9133

[26]   E. Tekin, E. Holder, V. Marin, B.-J. de Gans, U. S. Schubert, *Macromol. Rapid Commun.,* **2005**, *26*, 293-297.

[27]   H. J. Bolink, E. Coronado, R. D. Costa, E. Ortí, M. Sessolo, S. Graber, K. Doyle, M. Neuburger, C. E. Housecroft, E. C. Constable, *Adv. Mater.*, **2008**, *20*, 3910-3913.

[28]   R. D. Costa, E. Ortí, H. J. Bolink, S. Graber, C. E. Housecroft, M. Neuburger, S. Schaffner, E. C. Constable, *Chem. Commun.*, **2009**, 2029–2031.

[29]   S. Graber, K. Doyle, M. Neuburger, C. E. Housecroft, E. C. Constable, R. D. Costa, E. Ortí, D. Repetto, H. J. Bolink, *J. Am. Chem. Soc.,* **2008,** *130*, 14944–14945.

[30]   M. Mazig, A. König, *Eur. J. Org. Chem.,* **2007**, 3271–3276.

[31]   X.-B. Wang, J. E. Dacres, X. Yang, K. M. Broadus, L. Lis, L.-S. Wang, S. R. Kass, *J. Am. Chem. Soc.,* **2003**, 125, 296-304.

[32]   P. G. Hoertz, Y.-I. Kim, W. J. Youngblood, T. E. Mallouk, *J. Phys. Chem. B,* **2007***, 111(24)*, 6845-6856.

[33]   B. P. Sullivan, J. A. Baumann, T. J. Meyer, D. J. Salmon, H. Lehmann, A. Ludi, *J. Am. Chem. Soc.,* **1977**, *99(22)*, 7368-7370.

[34]   Y. Kita, H. Maekawa, Y. Yamasaki, I. Nishiguchi, *Tetrahedron*, **2001**, 57, 2095-2102.

7. Appendices

7.1 Crystal data

To find the right crystal structure and NMR spectra, the synthesized compounds are listed here with their names from the lab journal.

Compound 4: GS04	compound 6: GS08	compound 8: GS09
compound 10: GS10	compound 12: GS19	

7.2 NMR spectra

To complete this report on the following pages the measured and described ^{1}H spectra of compound 2 (GS02), compound 4 (GS04), compound 6 (GS08), compound 8 (GS09), compound 10 (GS10) and compound 12 (GS19) are listed.

The following is a list of the compounds in this work with their names from the lab journal and in the NMR spectra.

Compound 2:	GS02
Compound 3:	PR352
Compound 4:	GS04
Compound 5:	PR142
Compound 6:	GS08
Compound 7:	PR299
Compound 8:	GS08
Compound 9:	PR309
Compound 10:	GS10
Compound 11:	SG.079
Compound 12:	GS19
Compound 13:	JS1
Compound 14:	GS05
Compound 15:	GS05
Compound 16:	GS06
Compound 17:	JS9
Compound 18:	GS07
Compound 19:	bought
Compound 20:	GS11
Compound 21:	-
Compound 22:	GS14
Compound 23:	GS12, GS18
Compound 24:	GS13, GS15, GS16, GS17

GS02 in DCM (400 MHz)
asenger.029

GS04
500er NMR

F (d)
8.40

Q (d)
8.30

P (d)
8.19

H (d)
8.07

C (d)
8.54

D (t)
8.43

E (t)
8.26

O (d)
8.17

G (t)
8.11

I (d)
7.98

J (d)
7.55

K (t)
7.32

^{1}H NMR (500 MHz, DMSO) δ 9.25 (d, J = 8.4, 1H), 8.69 (d, J = 8.3, 1H), 8.54 (d, J = 8.2, 1H), 8.43 (t, J = 6.9, 2H), 8.40 (d, J = 7.8, 1H), 8.30 (d, J = 8.9, 1H), 8.26 (t, J = 8.8, 2H), 8.19 (d, J = 1.8, 2H), 8.17 (d, J = 4.9, 1H), 8.11 (t, J = 7.8, 1H), 8.07 (d, J = 7.8, 1H), 7.98 (d, J = 7.7, 1H), 7.55 (d, J = 9.2, 1H), 7.32 (t, J = 6.6, 1H), 6.74 (t, J = 7.4, 1H), 6.69 (t, J = 7.3, 1H), 6.28 (d, J = 7.4, 1H).

¹H NMR (500 MHz, DMSO) δ 8.98 (d, *J* = 8.5, 1H), 8.62 (d, *J* = 8.4, 1H), 8.29 (d, *J* = 8.2, 1H), 8.05 (s, 1H), 7.98 (d, *J* = 7.8, 1H), 7.94 (t, *J* = 7.8, 1H), 7.85 (d, *J* = 5.7, 1H), 7.39 (t, *J* = 8.0, 1H), 7.17 (t, *J* = 6.6, 1H), 7.07 (t, *J* = 7.5, 1H), 7.02 (d, *J* = 7.9, 2H), 6.97 (t, *J* = 7.5, 1H), 6.89 (s, 1H). 6.33 (d, *J* = 7.5, 1H), 3.75 (s, 3H).

GS08

GS09 in CD3CN (400 MHz)
gschneider.009/2

GS10
500 MHz, CDCN₃

B (s) 3.72   E (s) 3.34
A (s) 3.97   C (s) 3.57
D (s) 3.47
F (s) 1.47

¹H NMR (500 MHz, CD₃CN) δ = 3.97 (s, 1H), 3.72 (s, 1H), 3.57 (s, 1H), 3.47 (s, 1H), 3.34 (s, 1H), 1.47 (s, 1H).

GS19

C (d) 8.54   E (d) 8.31   G (dd) 8.14   H (t) 8.01
A (d) 8.86   B (d) 8.57   D (s) 8.41   F (d) 8.21   J (d) 7.91   K (d) 7.68   L (t) 7.24   M (t) 6.38   N (d) 5.80
I (d) 7.98

¹H NMR (500 MHz, CD₂Cl₂) δ 8.86 (d, J = 8.0, 1H), 8.57 (d, J = 7.5, 1H), 8.54 (d, J = 8.7, 1H), 8.41 (s, 1H), 8.31 (d, J = 7.6, 3H), 8.21 (d, J = 8.9, 1H), 8.14 (dd, J = 13.4, 6.5, 3H), 8.01 (t, J = 8.0, 1H), 7.98 (d, J = 8.0, 1H), 7.91 (d, J = 5.6, 1H), 7.68 (d, J = 9.1, 1H), 7.24 (t, J = 6.4, 1H), 6.38 (t, J = 10.7, 1H), 5.80 (d, J = 8.2, 1H).